

Paleoceanography and Paleoclimatology

RESEARCH ARTICLE

10.1029/2018PA003382

Special Section:

Climatic and Biotic Events of the Paleogene: Earth Systems and Planetary Boundaries in a Greenhouse World

Key Points:

- An interval largely devoid of carbonate extends across the middle and outer shelf in Maryland and New Jersey during the onset of the PETM
- We propose that the low carbonate interval was a result of shoaling of the CCD and lysocline to shelf depths during the onset of the PETM
- We consider the possibilities that shoaling was global but also regional, fueled by eutrophication and warming

Supporting Information:

- Supporting Information S1
- Figure S1
- Figure S2
- Figure S3
- Figure S4
- Figure S5

Correspondence to:

T. J. Bralower,
bralower@psu.edu

Citation:

Bralower, T. J., Kump, L. R., Self-Trail, J. M., Robinson, M. M., Lyons, S., Babila, T., et al. (2018). Evidence for shelf acidification during the onset of the Paleocene-Eocene Thermal Maximum. *Paleoceanography and Paleoclimatology*, 33, 1408–1426. <https://doi.org/10.1029/2018PA003382>









Received 5 APR 2018

Accepted 2 OCT 2018

Accepted article online 12 OCT 2018

Published online 21 DEC 2018

Evidence for Shelf Acidification During the Onset of the Paleocene-Eocene Thermal Maximum

Timothy J. Bralower¹ , Lee R. Kump¹ , Jean M. Self-Trail² , Marci M. Robinson² , Shelby Lyons¹, Tali Babila³ , Edward Ballaron⁴, Katherine H. Freeman¹, Elizabeth Hajek¹ , William Rush⁴ , and James C. Zachos⁴ 

¹Department of Geosciences, Pennsylvania State University, University Park, PA, USA, ²U.S. Geological Survey, Reston, VA, USA, ³Ocean and Earth Science, National Oceanography Centre Southampton, University of Southampton, Southampton, UK, ⁴Earth and Planetary Sciences, University of California, Santa Cruz, CA, USA

Abstract A transect of paleoshelf cores from Maryland and New Jersey contains an ~0.19- to 1.61-m-thick interval with reduced percentages of carbonate during the onset of the Paleocene-Eocene Thermal Maximum (PETM). Outer paleoshelf cores are barren of nannofossils and correspond to two minor disconformities. Middle paleoshelf cores contain a mixture of samples devoid of nannofossils and those with rare specimens characterized by significant dissolution (i.e., etching). The magnitude of the decrease in carbonate cannot be explained by dilution by clastic material or dissolution resulting from the oxidation of organic matter during early diagenesis. The observed preservation pattern implies a shoaling of the calcite compensation depth and lysocline to the middle shelf. This reduced carbonate interval is observed during the onset of the PETM on other continental margins raising the possibility that extreme shoaling of the calcite compensation depth and lysocline was a global signal, which is more significant than in previous estimates for the PETM. An alternative scenario is that shoaling was restricted to the northwest Atlantic, enhanced by regional and local factors (eutrophication from rivers and microbial activity associated with warming) that exacerbated the impact of acidification on the shelf.

1. Introduction

Modern marine and terrestrial environments are undergoing unprecedented rates of change as a result of human activities, exerting enormous pressure on ecosystems (e.g., Jackson et al., 2001; Jackson, 2008; Pandolfi et al., 2003). One of the most pervasive threats for marine organisms is ocean acidification resulting from air-to-sea transfer of anthropogenic CO₂ (e.g., Doney et al., 2009; Orr et al., 2005). More than a quarter of the CO₂ released into the atmosphere is absorbed by the ocean, lowering its pH and carbonate ion concentration (CO₃²⁻), hence the CaCO₃ saturation state. When saturation with respect to aragonite and calcite decreases below a certain level, calcifying organisms have more difficulty forming shells. Acidification is already impacting corals and is predicted to affect plankton such as coccolithophorids and foraminifera near the base of the food chain, as well as molluscs, in the next century (Fabry et al., 2008; Gattuso et al., 1998; Gazeau et al., 2007; Kleypas et al., 2006; Leclercq et al., 2000; Orr et al., 2005).

Greenhouse gas-driven abrupt warming events in deep time provide vital information about how the Earth and oceans will respond to climate change in coming centuries (e.g., see Honisch et al., 2012; Kump et al., 2009), including the ability of organisms to adapt to decreasing carbonate saturation. An ~200,000-year-long transient warming event approximately 56 million years before present, the Paleocene-Eocene Thermal Maximum (PETM), is viewed as possibly the best ancient model for the impact of future global warming and associated environmental change. The PETM involved a 5–8 °C warming of the surface and deep oceans (Kennett & Stott, 1991; Thomas & Shackleton, 1996; Zachos et al., 2003; 2005). This warming was driven by input of up to 10,000 Pg of CO₂ (e.g., (Dickens et al., 1995; Dickens, 2011; Gutjahr et al., 2017; Panchuk et al., 2008; Zeebe et al., 2009) with a significant portion released in less than 10,000 years (Cui et al., 2011; Röhl et al., 2007; Turner et al., 2017), as suggested by the magnitude and duration of the onset of the carbon isotope excursion (CIE). As such, the average rate of input of fossil carbon at the onset of the PETM was nearly an order of magnitude slower than it is today (e.g., Cui et al., 2011; Honisch et al., 2012; Ridgwell & Schmidt, 2010; Zeebe et al., 2016). Regardless, the sequence of the carbon cycle, climatic and environmental changes, and how they impacted organisms over the long term, provides important lessons for the future.

Warming and changes in nutrient distribution during the PETM had profound impacts on life in the oceans from plankton to reef builders (e.g., Bralower, 2002; Crouch et al., 2001; Gibbs, Bown, et al., 2006; Kelly et al., 1996, 1998; Raffi et al., 2009; Sluijs et al., 2007; Scheibner & Speijer, 2008a). Most of the carbon input at the onset of the event ended up in the deep ocean causing significant decreases in calcite saturation and at least a 2-km shoaling (Zachos et al., 2005) of the lysocline and calcite compensation depth (CCD). The *lysocline* is defined as the depth interval over which wt. % CaCO_3 drops below 80 wt. % (Broecker & Peng, 1982) and calcitic microfossil preservation in pelagic sediments declines due to dissolution (Berger, 1971). The top of the lysocline coincides with the depth below which calcite becomes undersaturated (Broecker & Peng, 1982). The CCD is the base of the lysocline, below which wt. % CaCO_3 is negligible, which for practical reasons is often defined as <10 or 20 wt. %, and typically where calcite is about 20% undersaturated (Broecker & Peng, 1982). Deep ocean acidification during the PETM is a hypothesized driver of the most significant deep-sea benthic foraminiferal extinction event in the last 90 million years (e.g., Thomas, 1998, 2007).

The impact of acidification during the PETM was dependent on both the quantity and rate of carbon released into the atmosphere (e.g., Cui et al., 2011; Gutjahr et al., 2017; Honisch et al., 2012). The surface ocean response is predicted to be relatively rapid, with a magnitude that depends heavily on the rate of input (Zeebe & Zachos, 2013). High-magnitude fluxes over decades and centuries in simulations lead to significant reductions in surface saturation state, but the same quantity of carbon released over 10^3 – 10^4 years has diminished impacts because of the ameliorating effects of biological pumping, mixing, seafloor dissolution, and the addition of alkalinity to the ocean from continental weathering (Archer et al., 1997; Kump et al., 2009; Walker & Kasting, 1992). Accordingly, surface ocean saturation would have decreased by a comparable amount to future saturation *projections* only with carbon input rate near the maximum expected for the PETM (Honisch et al., 2012; Ridgwell & Schmidt, 2010) or with short intervals of rapid carbon release (Frieling et al., 2016).

Because seafloor dissolution removes biogenic carbonate needed for analysis of assemblages and proxies, current evidence for surface ocean acidification in the PETM is elusive. Malformation and thinning of a small subgroup of calcareous nannoplankton species has been proposed as evidence for acidification (e.g., Bralower & Self-Trail, 2016; O'Dea et al., 2014; Raffi et al., 2009). Moreover, B/Ca and $\delta^{11}\text{B}$ isotope analyses of mixed-layer and thermocline dwelling planktic foraminifera, which provide a measure of ocean pH, suggest a moderate (0.2–0.4) decrease in pH over the peak of the CIE (Babila et al., 2016; Gutjahr et al., 2017; Penman et al., 2014), consistent with the lack of a widespread acidification response among planktonic calcifiers. However, as a result of the absence of carbonate, B/Ca and $\delta^{11}\text{B}$ isotope records likely omit the first ~1–2 kyr of the PETM when the impacts of acidification are likely to be most severe.

The response of the deep ocean is slower than the surface ocean given the slow rate of turnover. Moreover, the total amount of CO_2 is critical: simulations show that the saturation state reached a minimum at about 20 kyr after the onset of the event, at the end of carbon addition in the simulation, then slowly recovered (Cui et al., 2011; Gutjahr et al., 2017; Turner & Ridgwell, 2016). Deep-sea PETM sections, the focus of most paleoclimate investigations (e.g., Kennett & Stott, 1991; Zachos et al., 2003), are often condensed and characterized by bioturbation and winnowing, which obscures interpretations of shifts in the lysocline and CCD (e.g., Bralower et al., 2014). Sections deposited on the continental paleoshelf are, by comparison, more expanded and often include the vital earliest part of the event (e.g., John et al., 2008; Stassen et al., 2015). Even if more prone to breaks in deposition (e.g., erosional unconformities), PETM shelf sections generally have well-preserved fossil materials (Gibbs et al., 2013; O'Dea et al., 2014) and high sedimentation rates and therefore are more likely to record changes in ocean chemistry and biology that occurred over millennia at the onset of the event.

Here we investigate the dissolution history of the shallow ocean at paleoshelf sites from the U.S. Atlantic Coastal Plain that offer high temporal resolution along with high-fidelity biotic and geochemical proxy records of the earliest PETM. We explore the significance of an interval nearly devoid of carbonate at the base of the CIE that occurs across most of the shelf and is also found at sites on other continental margins.

2. Material and Methods

Sections from the subsurface of the Atlantic Coastal Plain from New Jersey and Maryland provide a transect from innermost shelf depths of ~50 m (Self-Trail et al., 2017) to outer shelf depths of ~150 m (Stassen et al.,

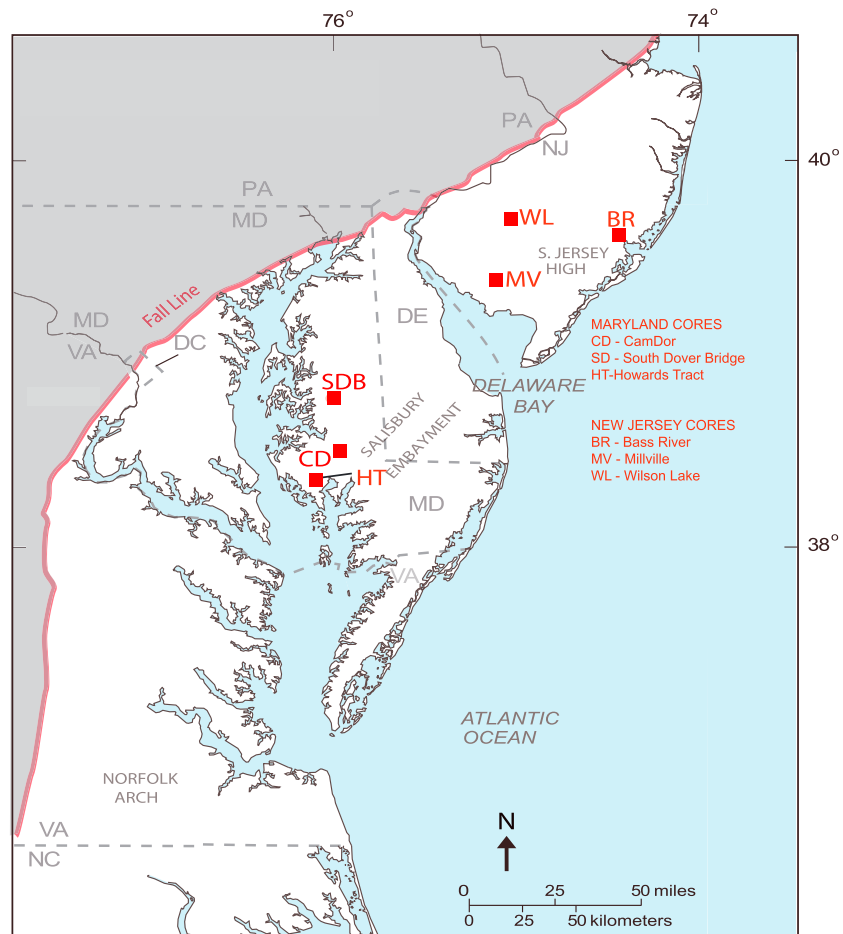


Figure 1. Map showing location of study sections on the Atlantic Coastal Plain.

2015). Here we investigate the onset of the PETM in three cores from New Jersey, including Bass River (BR), Millville (MV), and Wilson Lake (WL; (Cramer et al., 1999; John et al., 2008; Sluijs et al., 2007; Wright & Schaller, 2013) and three cores from Maryland, including Cambridge Dorchester Airport (Cam-Dor [CD]), Howards Tract (HT Core 2), and South Dover Bridge (SDB; Self-Trail et al., 2012; Figure 1 and Table 1). The study interval includes the transition from upper Paleocene glauconite-rich quartz sands of the Vincentown and Aquia formations to the silty-clay and clay of the Marlboro Clay (Cramer et al., 1999; Gibson et al., 1993, 2000; Harris et al., 2010). The sections are highly expanded with sedimentation rates in the early part of the PETM up to 50 cm/kyr (John et al., 2008; Self-Trail et al., 2017; Stassen et al., 2012). Samples were examined every 5 to 25 cm across the interval just below and within the onset of the CIE and at lower resolution in the upper part of the event.

Table 1

Depths of Key Intervals in Paleoshelf Sections Including Depths of Peak and Minimum $\delta^{13}\text{C}$ Values, Excursion Magnitude, Base and Top of the LCI, Base of the Marlboro Clay, and Base and Top of the Interval With Reddish Color (See Text for More Information)

Section	Peak $\delta^{13}\text{C}$ (m)	Min. $\delta^{13}\text{C}$ (m)	CIE Magn. (per mil)	Base LCI (m)	Top LCI (m)	Base Marlboro Clay (m)	Base red interval (m)	Top red interval (m)
BR	357.55	356.94	−2.93	357.29	357.1	357.2		
WL	109.95	107.5	−5.16	109.85	109.42	109.85		
MV	273.85	271.84	−4.53	273.68	273.54	274.14		
CD	224.22	222.05	−3.15	224.0	222.39	224.15	224.12	223.34
SDB	204.5	201.0	−3.15	203.93	202.4	203.91	203.99	202.81
HT	200.42	199.89	−10.61	200.31	198.42	200.41	200.41	199.03

Table 2
Depth of Datums (in m)

	Bass River	South Dover Bridge	Wilson Lake
Base <i>Rhomboaster</i> spp.	356.95	200.1	106.38
Base <i>D. salis</i> var. <i>acutus</i>	357.01	199.8	105.46
Base <i>D. salis</i> var. <i>araneus</i>	357.12	199.9	104.25
Base <i>D. salis</i> var. <i>vilosus</i>	357.12	200.1	106.68
Base <i>D. salis</i> var. <i>anartios</i>	357.12	200.9	107.9
Base T2l <i>D. multiradiatus</i>	357.2	202.7	109.23
Base T2l <i>D. salisburgensis</i>	357.2	202.1	108.91
Peak <i>Hornibrookina arca</i>	357.74	204.8	110.16
Peak <i>Calciosolenia aperta</i>	359.24	206.0	110.51

2.1. Biostratigraphy

The distribution of stratigraphically significant taxa in BR, WL, and SDB is based on previous studies (Bralower & Self-Trail, 2016; Gibbs, Bralower, et al., 2006; Self-Trail et al., 2012) and on additional observations of samples from BR. Smear slides were prepared using standard techniques and viewed in a light microscope at magnification of 1,250X. We compile the acmes of *Calciosolenia aperta* and *Hornibrookina arca* in the latest Paleocene and the first occurrences of the excursion nannoplankton in the early Eocene, including *Rhomboaster* spp., malformed *Discoaster multiradiatus* and *D. salisburgensis* (stage T2l of Bralower and Self-Trail, 2016), *Discoaster salisburgensis* var. *anartios*, *D. salisburgensis* var. *vilosus*, *D. salisburgensis* var. *araneus*, and *D. salisburgensis* var. *acutus* (Table 2).

2.2. Nannofossil Preservation

Counts of coccolith shield preservation are key to our interpretation. We observed the first 100 coccolith specimens in the light microscope and distinguished those that have entire rims not characterized by etching or fragmentation from those that are only partially preserved as a result of dissolution or possibly abrasion by bottom currents. We term this measure the whole shield index (WSI). Images of coccoliths with entire and partial rims used to calculate the WSI are shown in supporting information Figure S1. The higher the index, the better the coccolith preservation. We did not include nannolith genera such as *Discoaster*, *Fasciculithus*, and *Sphenolithus*, which are generally more resistant to dissolution. Where coccoliths are rare, we counted all specimens in five slide traverses, roughly 250 fields of view at 1,250X magnification.

2.3. Carbon Isotopes and Percent Carbonate

Bulk CaCO_3 C-isotope and % CaCO_3 data exist for most of the study sections (Cramer et al., 1999; John et al., 2008; Lyons et al., 2018; Self-Trail et al., 2012, 2017; Wright & Schaller, 2013). We measured % CaCO_3 on samples from the CD and HT sections and provide additional measurements of carbonate from samples from SDB. Carbonate analyses were carried out on a UIC Inc. coulometrics Coulometer at the University of California Santa Cruz with a precision of $\pm 0.05\%$. Results largely represent calcite but also likely include siderite where the latter mineral is abundant. Percent total organic carbon (TOC) measurements were carried out on a UIC Inc. Coulometer and a Costech ECS4010 Elemental Analyzer at Penn State with a precision of ± 0.1 . Stable isotope analysis of bulk carbonate of samples from CD and HT was carried out on a Kiel/MAT253 at the University of California Santa Cruz. Analytical precision based on replicate analyses of standards was better than $\pm 0.05\%$ for $\delta^{13}\text{C}$. All values are reported relative to vPDB. To provide ocean-wide context for the paleoshelf data set, we compiled % CaCO_3 and bulk carbonate C-isotope data at all available PETM sections from the deep sea and continental paleoshelf and paleoslope sites from the margins of the Tethys and the South Pacific (Pangaea Supplement Table). We estimated percent dissolution based on peak % CaCO_3 prior to the PETM combined with the lowest % CaCO_3 during the dissolution event following Broecker (1995; see supporting information).

2.4. Mineralogy

We observed abundant framboidal pyrite and other iron phases in all smear slides and grains of siderite in many. We counted the number of specimens in five smear slide traverses at 1,250X magnification to determine changes in abundance (see supporting information). Framboids and associated particles were observed in a FEI Nova NanoSEM 630 FE scanning electron microscope.

2.5. Grain Size

We measured the grain size of sediments from an extended interval in the CD, HT, and WL sections to determine how the sedimentology of samples impacts the carbonate record. Samples were disaggregated in water on a shaker table overnight and ultrasonicated before introduction into a Malvern Mastersizer 3000 particle sizer. Continuous sample aspiration allowed us to evaluate how flocculation impacted analysis; all analyses were run until D50 values were constant for multiple analyses. Samples were reanalyzed where there are abrupt shifts in records that could result from incomplete disaggregation.

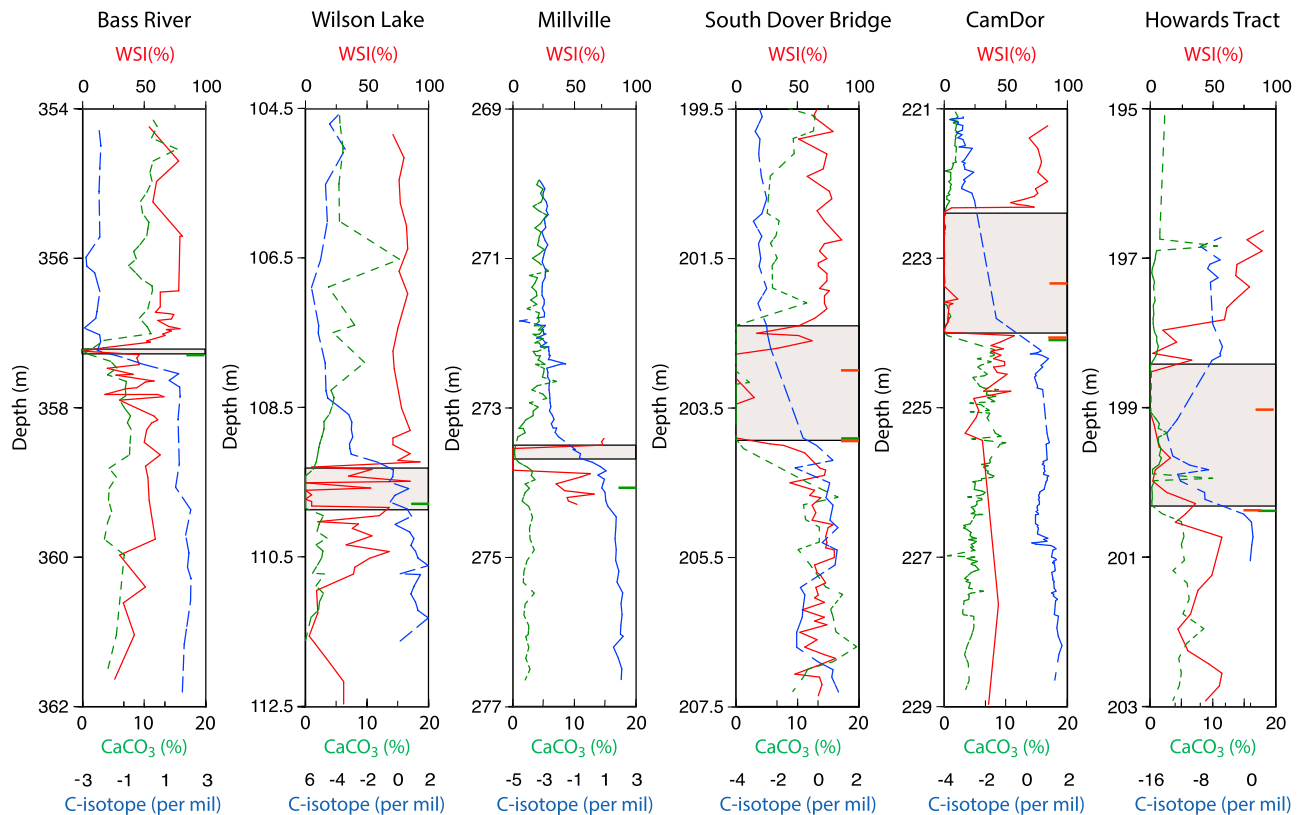


Figure 2. Definition of the low carbonate interval (LCI) shown in shaded gray area based on carbonate (green dashed curve) and the whole shield index (WSI; red curve) in the six study sites plotted with the bulk carbonate $\delta^{13}\text{C}$ curves (blue dashed curve). Small green ticks represent the base of the Marlboro Clay. Red ticks represent the base and the top of the interval with common hematite.

3. Results

We present bulk carbonate carbon isotope data for the CD and HT sections. Carbon isotopes from CD shows a gradual decline from 0.64‰ at 224.22 m to -3.16 ‰ at 222.07 m (Figure 2). Values remain low for the remainder of the study section. The record from HT shows a gradual decrease from 0.14‰ at 200.53 m to -11.61 ‰ at 199.89 m (Figure 2); after a minor increase, values decrease further to -13.34 ‰ at 199.34 m. This 13.5‰ shift is likely a result of the occurrence of siderite (Figure 5, Plates 11–18, and supporting information, Figure S2). Bulk carbonate isotope data for all other sections have been published elsewhere: BR and WL (John et al., 2008), MV (Wright & Schaller, 2013), and SDB (Self-Trail et al., 2012).

Carbonate content of samples from the New Jersey and Maryland paleoshelf sections is less than 20% (Figure 2). Average values for the Aquia and Vincentown Formations at the base of the study interval range from 2% (WL) to 12% (SDB). All of the study sites from Maryland and New Jersey show a prominent interval in which carbonate decreases to close to 0% during the onset of the CIE (Figure 2) at the base of the Marlboro Clay. This is termed the low carbonate interval (LCI). Minimum % CaCO_3 in the LCI are 0% in all sections, but each section has sporadic samples with higher % CaCO_3 (up to 2.75% at HT). Definition of the base of the LCI is based on the stratigraphically lowermost level of 0% CaCO_3 , except at BR where it is based on the decrease in % CaCO_3 . The top of the LCI is defined by the recovery of CaCO_3 values and is somewhat subjective, especially at BR, SDB, and HT. The thickness of the LCI varies from 0.19 m at BR (357.1 to 357.29 m) up to 1.61 m at CD (222.39 to 224.0 m; Table 1). The transition of the LCI with surrounding sediments is relatively abrupt, corresponding to <10 cm in all sections. In all sections, samples immediately above the LCI contain higher % CaCO_3 than those immediately below it (Figure 2). Unpaired t tests show a highly significant difference between CaCO_3 values in the LCI and surrounding sediments in all sections except HT (Table 3).

Table 3Unpaired *t* Tests of Composition of Samples From LCI Compared to Samples Outside the LCI

Value	Wilson Lake Mean	STD	Bass River Mean	STD	Millville Mean	STD	CamDor Mean	STD	SDB Mean	STD	HT-2 Mean	STD
CaCO ₃ LCI	0	0	1.83	1.79	0.46	0.31	0.14	0.24	0.16	0.58	1.15	0.81
CaCO ₃ NLCI	3.64	2.75	8.38	2.77	3.6	1.19	4.65	2.29	10.03	4.17	2.37	2.63
<i>P</i> value	0.0025*		0.0002*		0.0001*		0.0001*		0.0001*		0.1028	
TOC LCI	0.48	0.13	NA		0.48	0.05	0.62	0.19	0.47	0.16	0.65	0.2
TOC NLCI	0.33	0.15	NA		0.42	0.11	0.73	0.32	0.26	0.13	0.52	0.23
<i>P</i> value	0.0326		NA		0.2195		0.1781		0.0003*		0.1536	
Pyrite LCI	373	349.33	149.67	79.12	417.67	204.57	414.65	745.46	182.71	197.96	574.11	220.02
Pyrite NLCI	168.75	170.26	84.65	86.49	489.17	172.69	492.9	357.92	205.86	199.8	868.92	479.29
<i>P</i> value	0.1094		0.2255		0.4466		0.6732		0.357		0.0155	
Pyr. Oxidation LCI	39.2	34.8	74.5	11	66.83	8.28	29.08	15.09	33.83	26.21	24.38	7.85
Pyr. Oxidation NLCI	28.83	15.77	67.83	14.37	43.88	14.61	38.69	22.85	19	4.66	22.93	5.68
<i>P</i> value	0.335		0.4568		0.0049*		0.2314		0.0413		0.6168	
Siderite LCI	16.17	21.25	2	2.65	0.67	0.82	0	0	0.33	0.82	452.89	466.15
Siderite NLCI	18.08	17.04	9.5	16.55	1	1.51	1.46	3.45	1.87	3.38	51.71	89.52
<i>P</i> value	0.8381		0.447		0.6355		0.1403		0.2921		0.0014*	

Note. *P* values shown in bold are significant; values shown with asterisks are very significant. LCI = low carbonate interval; NLCI = non-low carbonate interval (intervals analyzed shown in Figure 2).

Samples from the LCI contain rare, heavily etched nannofossils indicative of dissolution, and we estimate the WSI from limited number of specimens. Where coccoliths are absent (often where % CaCO₃ is 0), the WSI is assumed to be 0%. The sections show relatively constant or slightly increasing WSI values below the CIE with values mostly less than 60% and a marked increase at the top of the LCI (Figure 2) with values between 60% and 80%. Samples directly above the LCI have higher WSI values, indicating preservation that is superior to directly below it. This trend has also been observed in previous fragmentation counts at WL (Gibbs, Bralower, et al., 2006). The WSI shows more intersample variability than carbonate records for two reasons: (1) minor changes in etching of samples can lead to wholesale changes in the WSI that do not correspond to significant changes in carbonate and (2) the WSI data are generally higher in resolution than the carbonate data.

Data from CD, HT, and WL show a gradual decline in average grain size across the transition from the Aquia and Vincentown Formations to the overlying Marlboro Clay (Figure 7). The LCI shows gradually increasing grain size in all three sections from bottom to top but is not significantly coarser than surrounding levels.

The LCI lies above the acmes of *C. aperta* and *H. arca* at BR, SDB, and WL (Table 2 and Figure 3). At BR the first occurrences (FOs) of malformed *D. multiradiatus* and *D. salisburgensis* (T2I) and of *D. salisburgensis* var. *anartios* and *D. salisburgensis* var. *araneus* all lie within the LCI; the former two datums lie at 357.2 m, and the latter two datums lie at 357.12 m (Table 2 and Figure 3). At SDB, the FO of malformed *D. multiradiatus* (T2I) lies within the expanded dissolution zone but here and at WL, the other datums are distributed over a 2- (SDB) to 5-m (WL) interval. Thus, we interpret two minor disconformities at 357.2 and 357.12 m within the LCI at BR.

Pyrite framboids are common in all sections but generally more abundant at CD and HT than elsewhere (Figures 4, 5, Plates 1–3, and 6, Plates 1–6). There is a noticeable increase in the abundance of framboids at the top of the LCI in all sections except for BR. These materials are often partially altered to hematite (reddish color) and, possibly, jarosite (yellow to orange color; Figure 5, Plates 4 and 5, and supporting information Figures 3 and 4). In the three Maryland sections, the LCI begins close to the transition to sediment with reddish hue (Figure 2), which appears to represent an increase in the abundance of finely disseminated hematite (Figure 5, Plates 9 and 10). However, the LCI extends several decimeters above the reddish interval. The three New Jersey sections have less finely disseminated hematite. The sample from the peak of the LCI at BR contains abundant quartz. In all sections the abundance of framboids decreases slightly near the base of the LCI and increases toward the top, although the exact timing of these changes relative to the boundaries of the LCI varies from section to section (Figure 4). Smear slide observations show that foraminiferal chambers are often the site of framboid growth (Figure 5, Plates 6 and 7). Numerous samples at WL, and especially HT, have abundant siderite (Figure 5; Plates 11–18; Self-Trail et al., 2017); this mineral is relatively rare in the other

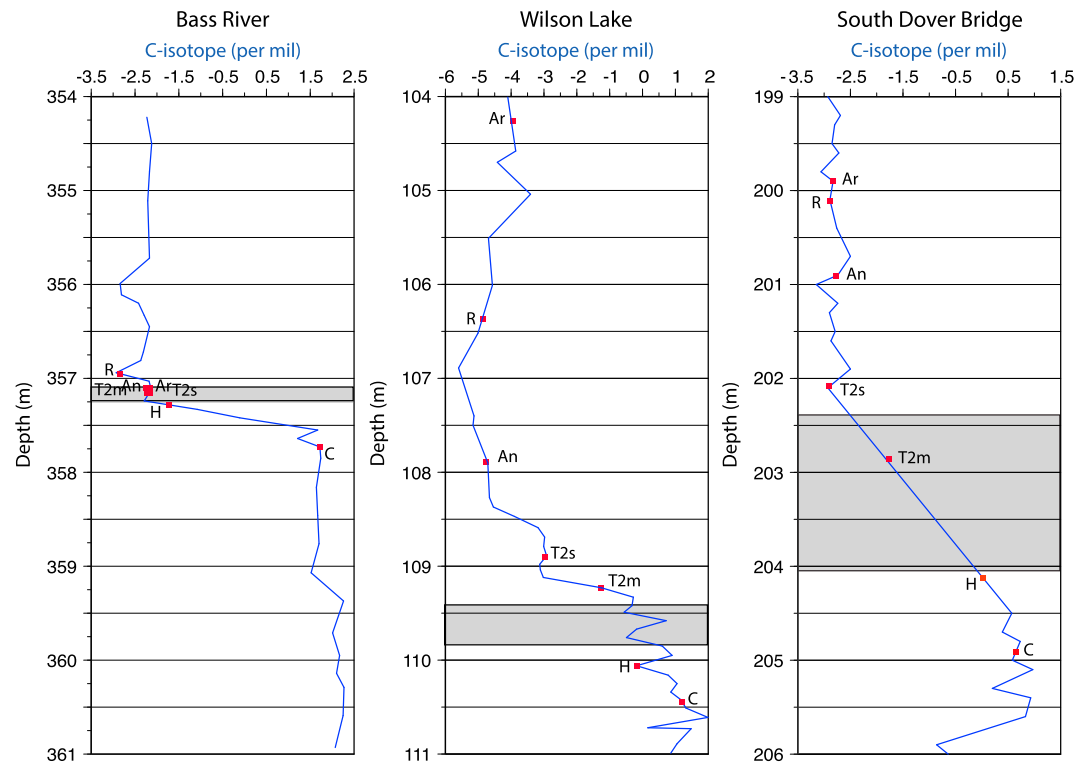


Figure 3. Stratigraphy of the low carbonate interval at Bass River, Wilson Lake, and South Dover Bridge. Included are the bulk carbonate isotope stratigraphy and significant biostratigraphic events including the acme of *Calcosolenia aperta* (C) and the acme of *Hornibrookina arca* (H). Also shown are the base stage T2I *D. salisburgensis* (T2s), base T2I *D. multiradiatus* (T2m), base *D. salisburgensis* var. *araneus* (Ar), and base *D. salisburgensis* var. *anartios* (An; all defined by Bralower & Self Trail, 2016), and base *Rhomboaster* spp. (R). Datums compiled in Table 2. Shaded grey area is the low carbonate interval.

sections (supporting information Figure 2). Unpaired *t* tests do not show consistent, statistically significant differences in the abundance and oxidation of pyrite, the abundance of siderite, or %TOC between the LCI and surrounding samples (Table 3). The LCI shows significantly higher %TOC at WL and SDB and significantly higher abundance of siderite at HT; it also shows lower abundance of pyrite and more oxidized pyrite at MV and SDB. There is considerable variation in grain size between the three sections; the LCI is coarsest at CD and finest at WL. At all sites the LCI has grain size intermediate between the Aquia and the upper part of the Marlboro Clay (Figure 7); at CD the interval shows a slight coarsening upward trend and a sharp drop in grain size 30 cm above the LCI.

4. Discussion

Calcium carbonate deposition is highly sensitive to input of CO_2 ; thus, the onset of the PETM is marked by a sharp decrease in carbonate in marine sedimentary archives (e.g., Honisch et al., 2012; Zachos et al., 2005). Yet the paucity or absence of carbonate makes understanding dissolution an elusive topic. Where minor or moderate carbonate remains, these materials provide clues to the processes that controlled dissolution. However, where extensive dissolution has led to the removal of most, if not all, carbonate, the extent and causes of dissolution are much more difficult to constrain.

4.1. The WSI: A Measure of Dissolution

The percentage of foraminifera that are broken or fragmented, the foraminiferal fragmentation index, hereafter referred to as the FFI, is well established as a measure of dissolution on the seafloor and during burial (e.g., Thunell, 1976). The FFI requires samples to be washed and thus is relatively labor intensive. Moreover, disaggregation of indurated sedimentary rocks increases the FFI. The WSI is determined on smear slides, which involve less preparation; such slides can be made on relatively indurated materials that

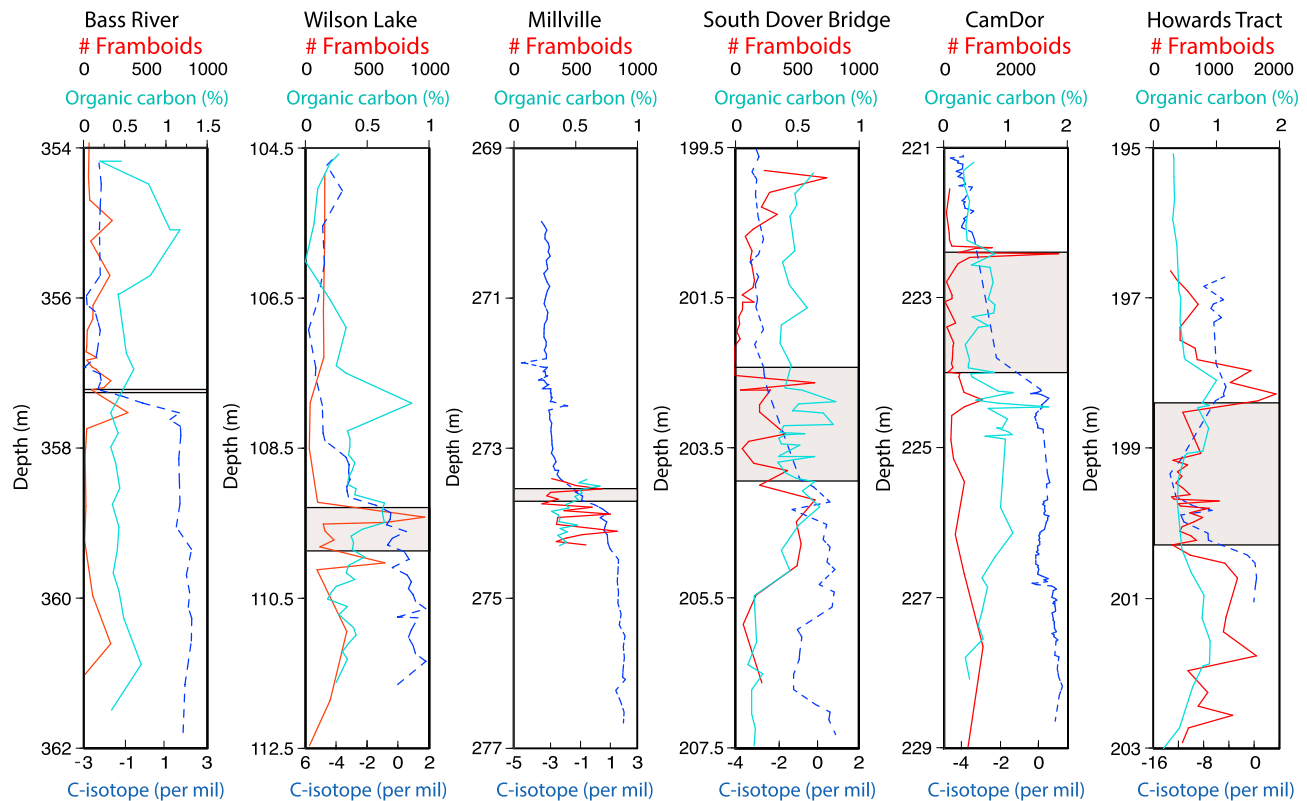


Figure 4. Abundance of pyrite framboids in five slide traverses (plotted in red; note the different scale for CD and HT) plotted with total organic carbon (%) in light blue) and bulk carbonate $\delta^{13}\text{C}$ curves (dark blue dashed line). Shaded gray area is the LCI.

disaggregate in water. A comparable measure was previously employed by Gibbs, Bralower, et al. (2006) and Self-Trail and Seefelt (2005) from various coastal plain cores to assess changes in nanofossil preservation.

The WSI is thus proposed as a measure of dissolution at the seafloor during the PETM through early burial. Although some of the partial specimens could be a result of abrasion on the seafloor during the deposition of the coarser-grained Aquia and Vincentown formations, dissolution is most likely responsible for the majority of the incomplete coccoliths in the lower energy Marlboro Clay. The WSI shows an abrupt decrease to zero in the LCI at all sections but shows more variability throughout this interval at HT and WL (Figure 2). In these sections, minor increases in the WSI within the LCI reflect samples with rare nanofossils suggesting sporadic carbonate preservation. The occurrence of sporadic, heavily etched nanofossils in these sections and the gradual changes in WSI at the base and top of the LCI in most sections strongly indicate dissolution as the major control on WSI values.

4.2. Origin of the Low Carbonate Interval

In this section we explore several hypotheses for the origin of the LCI at the six study sites. A correlative event is present in the Ancora and Clayton cores, which were also located on the New Jersey middle paleoshelf (Pangaea Supplement Table). Assuming that carbonate production rates did not change across the LCI, an assumption that is difficult to evaluate, the decrease in % CaCO_3 suggests reduced biogenic carbonate accumulation of up to 100% (Pangaea Supplement Table). A significant part of the carbonate decrease may result from dilution by terrigenous material corresponding to the pulse of mud that swept across the shelf at the onset of the PETM. Alternatively, the LCI may represent an episode of dissolution on the outer and middle paleoshelf coincident with the onset of the event. This dissolution may be regional or part of a global event, and it may be associated with shoaling of the CCD and lysocline to paleoshelf depths or removal of CaCO_3 during early burial diagenesis. Here we weigh evidence for each of these possibilities (or some combination of them) and test them with the global data set.

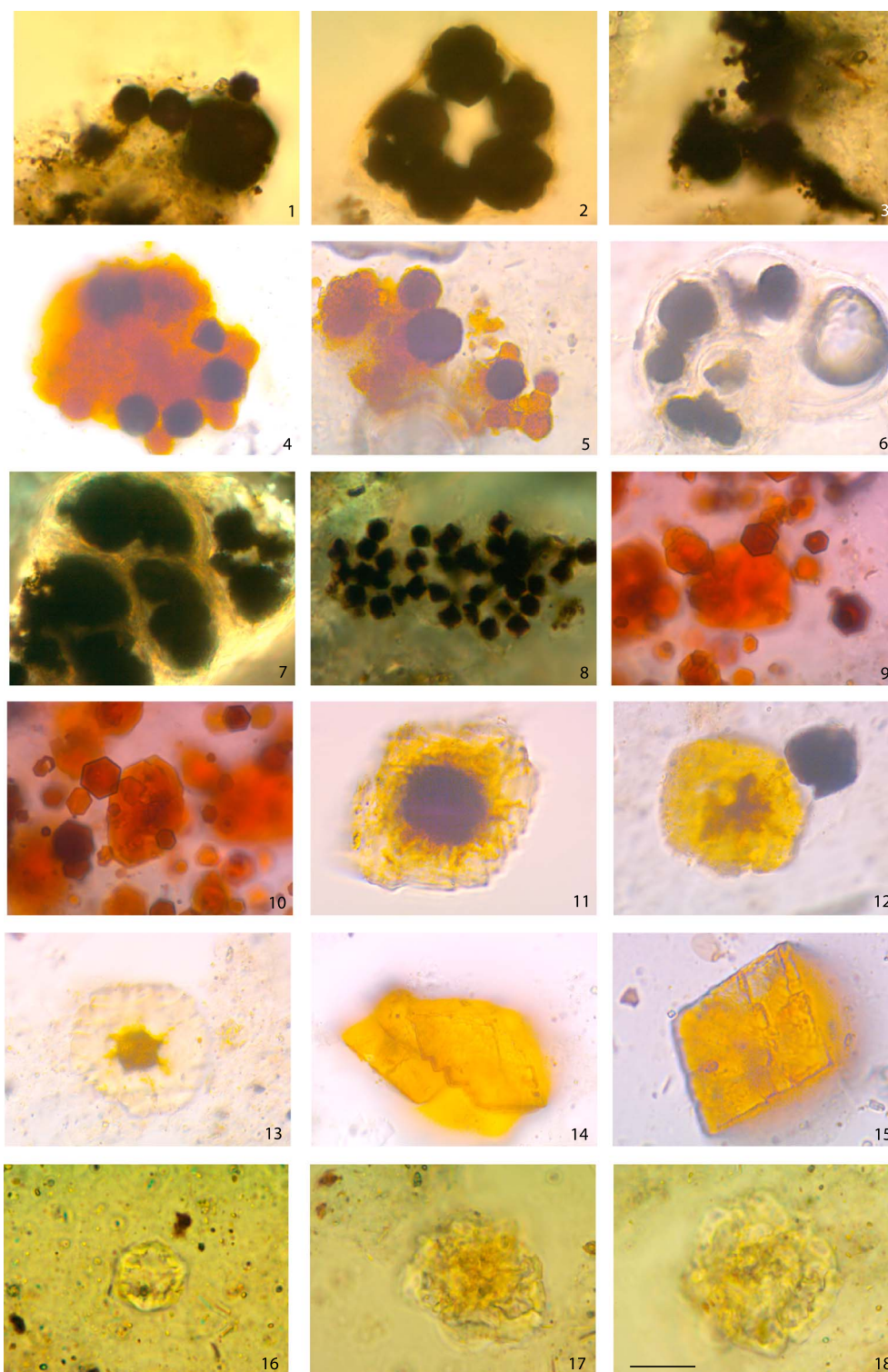


Figure 5. Plates 1–18: Brightfield light photographs except those indicated. 1. Pyrite framboids, sample HT 201.76 m. 2. Pyrite framboids inside a chamber sample HT 201.76 m. 3. Pyrite framboids, sample HT 201.76 m. 4. Oxidized pyrite framboids, sample WL 110.3 m. 5. Oxidized pyrite framboids, sample BR 356.80 m. 6. Pyrite framboids inside a foraminifer chamber, sample BR 357.10 m. 7. Pyrite framboids inside a foraminifer chamber in cross-polarized light, sample HT 202.43 m. 8. Finely dispersed pyrite, sample HT 202.43 m. 9 and 10. Hematite, sample HT 205.77 m. 11. Siderite with internal pyrite framboid, sample WL 107.29 m. 12. Siderite with remnants of internal pyrite framboid WL 105.77 m. 13. Siderite with oxidized internal pyrite framboid, sample WL 106.68 m. 14. Siderite, sample WL 110.03 m. 15. Siderite, sample WL 110.03 m. 16. Siderite grain with internal etching, sample HT 196.90 m. 17. Siderite grain with internal etching, sample HT 199.74 m. 18. Siderite grain with internal etching, sample HT 199.74 m. Scale bar bottom right is 5 μm .

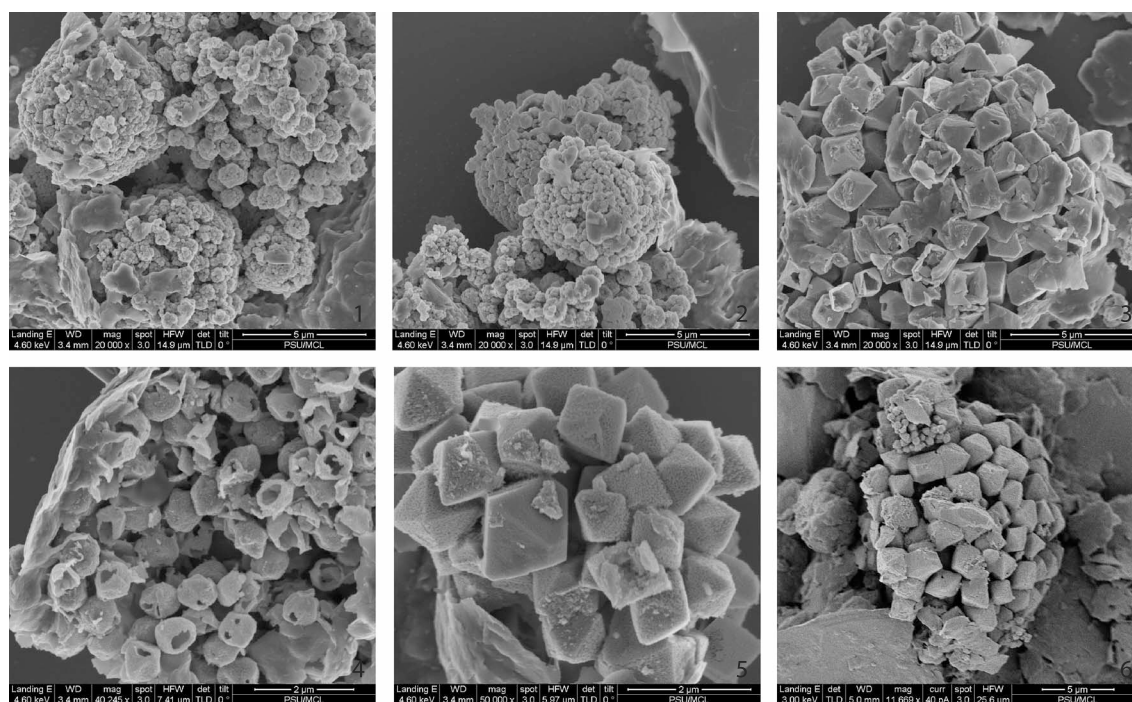


Figure 6. Plates 1–6: Scanning electron micrographs of framboidal pyrite. 1. Sample CD 222.39 m. 2–6. Sample CD 222.35 m. Scale bars at bottom right of each figure.

4.2.1. The Impact of Dilution on Interpretation of the LCI

The onset of the PETM coincided with a transgression (e.g., Sluijs et al., 2008) changing sedimentation patterns across the shelf. Typically, transgressive system tracts lead to sediment starvation on the middle and outer shelf as the locus of deposition moves landward (e.g., Loutit et al., 1988). However, the deposition of the Marlboro Clay involved a massive pulse of mud and fine silt at the front of a coastal delta in the Salisbury Embayment (e.g., Kopp et al., 2009; Self-Trail et al., 2017) and it is likely that sediment supply increased across the shelf. Thus, we begin by considering the possibility that the LCI at the base of the Marlboro Clay represents dilution of the flux of planktonic and benthic microfossils by clastic material.

In all records, grain size decreases below the base of the LCI and there is not a distinct grain size anomaly in this interval that might be expected for a pulse of terrigenous materials (Figure 7); the silty grain size at CD and HT compared to surrounding intervals is likely a result of the near-complete absence of coccoliths. Moreover, biostratigraphy suggests that the LCI represents a substantial amount of time (Figure 3), in contrast to some interpretations of the onset of the CIE (Kent et al., 2017; Wright & Schaller, 2013).

Dilution with terrigenous material should cause a decrease in the content of biogenic materials, including organic carbon and carbonate. Unpaired *t* tests do not show a significant difference between the Corg content of sediments in the LCI and those surrounding it. Dilution can only explain these similarities if the production of Corg increased in the LCI as has been proposed by (John et al., 2008). Although the onset of the PETM corresponded to eutrophication (e.g., Gibbs, Bralower, et al., 2006; Sluijs et al., 2007), there is no evidence that the LCI was unique from the remainder of the PETM in terms of productivity. Carbonate is significantly lower in the LCI in all sections except for HT than in surrounding intervals (Table 3). Dilution can potentially explain much or all of the decrease in %CaCO₃, but, crucially, it does not support dissolution coincident with the drop in the WSI.

Other microfossil groups do not show decreases that would be expected with dilution. Dinoflagellates are found throughout the LCI at BR and WL (Sluijs et al., 2008), and agglutinated benthic foraminifera are common in samples from SDB and WL (Robinson & Spivey, this volume; Stassen et al., 2015). The occurrence of agglutinated but not calcareous benthic foraminifera also indicates that the LCI resulted primarily from dissolution of carbonate rather than sediment dilution.

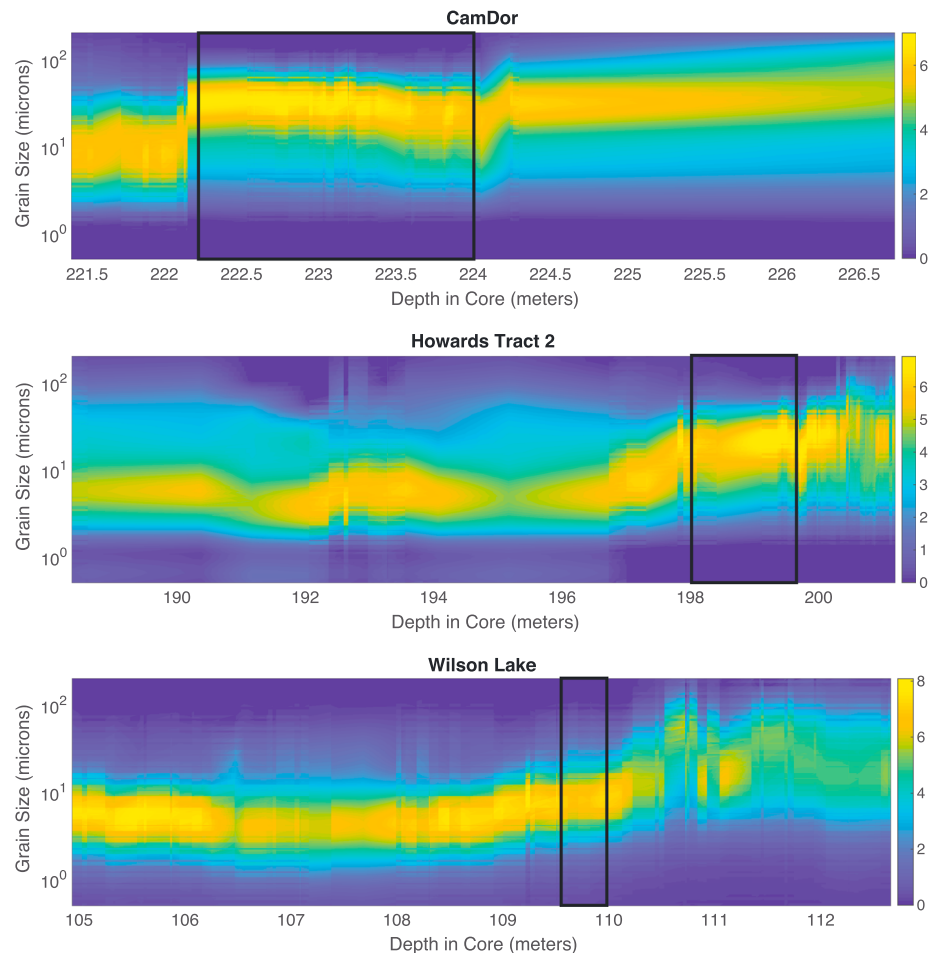


Figure 7. Grain size of samples from CamDor, Howards Tract and Wilson Lake plotted versus depth. Data are presented as density plots of grain size. Note grain size is plotted on logarithmic scale. Color density scale for each plot is shown at right. Box indicates location of the LCI.

Although the character of individual records is expected to differ due to local variations in sedimentation and erosion (Trampush & Hajek, 2017), the broad similarity of carbonate trends across the shelf suggests that the association between the loss of carbonate and the C-isotope excursion is robust. Increased clastic sediment flux may have contributed to reduced % CaCO_3 in these sections; however, the presence of the LCI in the most distal location (BR), which should be least impacted by dilution effects, suggests that the loss of carbonate was shelf wide and may have been independent of clastic supply. While the impact of clastic dilution cannot be ruled out, dilution is generally inconsistent with the absence of changes in the concentration of Corg. This absence of calcareous benthic foraminifera in most sediments, combined with the presence of agglutinated benthic foraminifera and the decline in the WSI, is strong evidence that dissolution, not dilution, is the main cause of the LCI.

4.2.2. Evidence for Carbonate Dissolution During Diagenesis and After Core Recovery

Dissolution of carbonate may have occurred along with the oxidation of organic matter during early burial (Froelich et al., 1979). The onset of the PETM is associated with an increase in surface ocean productivity on the paleoshelf (Gibbs, Bralower, et al., 2006; Self-Trail et al., 2012) and possibly an increase in the flux of organic matter to the seafloor from either allochthonous or contemporaneous sources (Schneider-Mor & Bowen, 2013). Thus, there is potential for dissolution of organic matter during early diagenesis. To dissolve 10 wt% CaCO_3 solely from organic matter oxidation during diagenesis, 1.2 wt% of organic carbon would need to be oxidized to CO_2 . While this is not impossible, most sites contain <1% TOC for the entire record, and only two of five sections show a statistically significant increase in % TOC in the LCI compared to surrounding units

with excellent carbonate preservation (Figure 4 and Table 3). For carbonate in the LCI to be dissolved from organic matter oxidation alone, %TOC would need to double within the LCI through an increase in productivity or preservation and then effectively be respired to CO_2 within the sediments. Our records do not provide sufficient evidence (i.e., hypoxia or high productivity) to explain increased organic matter delivery to and oxidation within sediments localized in the LCI. Moreover, there is no evidence for a distinct source of more reactive organic material coincident with the LCI (Lyons et al., 2018; Schneider-Mor & Bowen, 2013). While it is not impossible, we rule out organic matter oxidation during diagenesis as a probable cause for carbonate dissolution on the shelf. Bioturbation tends to buffer pore water alkalinity, and this could limit dissolution during early burial (Panchuk et al., 2008). Another possibility is that freshwater input lowered sulfate concentrations thereby decreasing calcite saturation during sulfate reduction (e.g., Meister, 2013). However, the normal marine fauna and flora on either side of the dissolution zone is evidence for typical marine salinity sulfate levels, and the shallowest shelf section at Mattawoman Creek-Billingsley Road, presumably with the largest freshwater influence, contains moderately well preserved carbonate (Self-Trail et al., 2017) in this interval.

Oxidation of pyrite can lead to dissolution of carbonate (e.g., Aller, 1988). Hematite, and possibly jarosite, replaced whole framboids and grew on framboid rims (Figure 5, Plates 4, 5, 9, and 10) indicating that oxidation has occurred. The presence of abundant framboids with clear evidence for oxidation raises the possibility that dissolution could have occurred long after deposition through interaction with oxidizing groundwaters, or after drilling and core recovery, which has previously been documented from coastal plain sediments (Seefelt et al., 2015; Self-Trail & Seefelt, 2005). The Aquia Formation is a regional aquifer, and the Marlboro Clay is known to be an aquiclude (Andreasen et al., 2013); even silty samples from the LCI in Maryland (Figure 7) were dry when recovered. Nevertheless, two pieces of evidence suggest that pyrite oxidation has led to CaCO_3 dissolution: (1) clusters of pyrite framboids appear to have grown within foraminiferal chambers (Figure 5, Plates 6 and 7) that subsequently dissolved (Figure 5, Plate 4) and (2) the proportion of oxidized framboids is lower in slides made immediately after coring at CD than those made after several years of core storage (supporting information Figure 4). However, other evidence suggests that this dissolution is limited: (1) most slides from the LCI prepared immediately after coring also are void of nannofossils at CD, as they are at HT and SDB; (2) there are numerous samples with significant amounts of oxidized framboids and well-preserved nannofossils and numerous LCI samples with unaltered pyrite (Figure 5, Plates 1–3 and 8, and supporting information Figures S4, and S5); and (3) the most oxidized framboids occur at BR (Table 3), which arguably has the best carbonate preservation. The reddish colored interval in the three Maryland study sections appears to represent finely disseminated hematite (Figures 2 and 5, Plates 9 and 10). This hematite could be detrital in origin or derived via oxidation of finely disseminated pyrite. However, the boundaries of the reddish interval and the LCI do not correlate (Figure 2 and Table 1). In summary, it is highly likely that oxidation of organic matter and pyrite led to at least some carbonate dissolution; however, the available evidence indicates that these diagenetic processes are not unique to the LCI. Thus, in the following, we consider primary origins for the LCI.

4.2.3. Evidence for CCD and Lysocline Shoaling

In the modern ocean, the lysocline and CCD occur at depths well below the shelf-slope break; incursions onto the continental shelf have rarely been documented in Earth history (an exception is the study of Pennsylvanian cyclothems by Heckel et al., 1994). Except on carbonate platforms, CaCO_3 percentages on continental shelves are significantly lower than in the deep sea, so assigning a lysocline depth is challenging. Moreover, coccoliths in upper Paleocene paleoshelf sediments are generally moderately fragmented, possibly due to abrasion in the high-energy conditions. However, there is further decline in both % CaCO_3 and WSI values in the LCI (Figure 2) and we use the coincidence of the decreases to define the lysocline and CCD on this PETM paleoshelf. For this discussion, we choose 90% dissolution to define the CCD.

Two minor disconformities coincide with upper part of the LCI at the outer paleoshelf BR site. The upper 8 cm of the LCI at this location is equivalent to ~3 m at SDB and ~5 m at WL (Table 2 and Figure 3). This highly condensed section could be a result of sequestration of sediment on the inner shelf during the PETM transgression (Harris et al., 2010). Sequestration of detrital sediment on the inner shelf would result in a highly condensed, but still continuous, section on the outer shelf dominated by the biogenic sediment fraction. However, sea level remained high for most of the PETM and the BR section appears complete for much of the peak and early recovery parts of the event (Stassen et al., 2015). The disconformities at 357.2 and 357.12 m are associated with the middle of the LCI (357.29 to 357.10 m) at BR and carbonate content

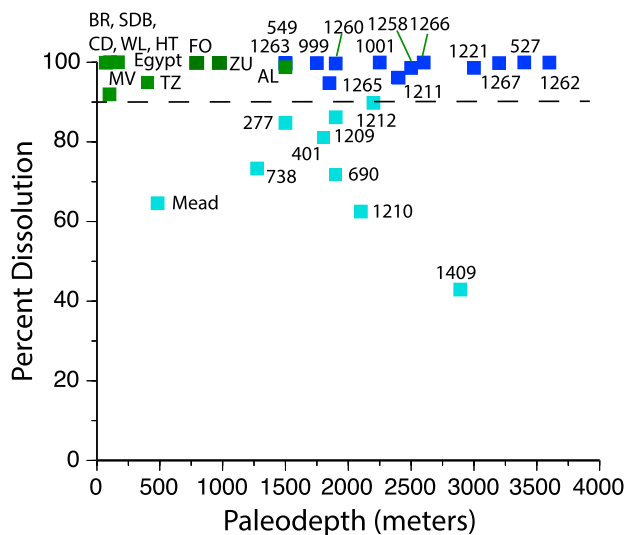


Figure 8. Percent dissolution (calculated after Broecker, 1995) plotted against paleodepth (see Pangaea Supplement Table for sources of paleodepth interpretation). Dashed line represents 90% dissolution signifying the lower limit of the CCD. Green are shelf sections, dark blue are sections with >90% dissolution interpreted as lying below the CCD, and light blue are sites characterized by <90% dissolution as a result of bioturbation, incomplete core recovery at the base of the PETM, or faulted outcrop (Mead). See text for discussion. Sites: BR-Bass River, CD-CamDor, HT-Howards Tract, MV-Millville, SDB-South Dover Bridge, WL-Wilson Lake, AL-Alemedilla, Spain, ZU-Zumaya, Spain; FO-Forada, Italy; TZ-Tanzania Core TDP-14, Egypt-Duwi Section, Mead Stream, NZ.

increases at the top of the interval. The only completely barren samples are found in the middle of the LCI (at 357.19 and 357.22 m); all other samples in this interval are moderately etched. This suggests that dissolution was syndepositional (see Bralower et al., 2014, for terminology); postdepositional, diagenetic burndown dissolution would be signified by a unconformity below the barren interval at the base of the LCI. We interpret the apparent unconformities at this outer shelf location (140–150-m water depth) as the result of dissolution at the seafloor in the lowermost part of the lysocline or below the CCD.

The LCI in the middle shelf sections at MV, WL, CD, HT, and SDB (120–130-m water depth) is not associated with apparent hiatuses. Like BR, this interval ranges from 78% to 100% dissolution with sporadic samples with heavily etched nannoplankton (supporting information Figure S5). Thus, we also interpret dissolution in these sections to have occurred in the lower part of the lysocline or below the CCD.

4.2.4. The Case for Global Shoaling of the CCD and Lysocline to the Continental Shelf

Next, we integrate results from the shelf transect to carbonate data from a global database of PETM sections (Pangaea Supplement Table) to determine if the proposed CCD and lysocline shoaling of the paleoshelf of the Atlantic Coastal Plain is part of a global trend. The global data set shows 90%–100% dissolution at sites from a broad range of paleodepths (Figure 8 and Pangaea Supplement Table). All complete sections below 2,500-m paleodepth are marked by 100% dissolution (dark blue symbols in Figure 8). Moreover, paleoshelf and paleoslope sites from Egypt, Italy, Nigeria, Spain, and Tanzania ranging from 100 to 1,500-m paleo-water-depth, similar to or much deeper than the sites investigated on the

Atlantic Coastal Plain, are also characterized by ~100% dissolution during part of the CIE (Alegret et al., 2009; Aze et al., 2014; Dupuis et al., 2003; Frieling et al., 2017; Giusberti et al., 2007; Lu et al., 1998; Schmitz et al., 1997; green symbols in Figure 8). The LCI in Nigerian and Tanzanian sections has been attributed to temperatures during the height of the PETM that exceeded the tolerance of planktonic calcifiers (Aze et al., 2014; Frieling et al., 2014, 2017). Our results suggest that dissolution could have also contributed. Shallow water communities in carbonate platforms including coralline reefs showed significant decline in the Paleocene-Eocene boundary interval, also likely largely due to heat stress (Scheibner & Speijer, 2008a). However, eutrophication and acidification during the PETM also may have played a role (Scheibner & Speijer, 2008b). The only paleoshelf section that is expanded without apparent dissolution is Site 1172 on the Tasman Rise where bulk Ca data show a slight increase during the PETM suggesting a lack of dissolution (Sluijs et al., 2011). However, samples through the PETM are barren of nannofossils and foraminifera suggesting dissolution, possibly associated with shoaling of the lysocline, and reprecipitation.

Evidence for >90% dissolution, the threshold that we use to define the CCD, from another group of sites ranging from 1,100 to 2,400-m paleodepth is less clear, however (light blue symbols in Figure 8 denotes sites with <90% dissolution). Carbonate values above zero during the onset of the PETM (and dissolution percentages 71%–90%) may be a result of the combination of slow sedimentation, bioturbation, and possibly winnowing, which could have masked a thin 90%–100% dissolution zone (e.g., Bralower et al., 2014). At other oceanic sites, including Sites 401, 689, and 738, the base of the event was incompletely recovered by coring as it was at deeper Site 1409 (Pangaea Supplement Table). Some land sections in this depth range contain expanded PETM records but with complications. At an expanded paleoslope section from the continental margin of New Zealand (Mead Stream; 78% dissolution), the PETM lies above a faulted interval and the published records (Hollis et al., 2005; Slotnick et al., 2012) may contain a gap at the base of the event.

Although previous studies have used these sites to constrain the upward migration of the lysocline and CCD to below 1,000 m or so (Alegret et al., 2009; Colosimo et al., 2006; Giusberti et al., 2007; Panchuk et al., 2008; Zachos et al., 2005; Zeebe et al., 2009), expected variability of carbonate contents even below the CCD

(Broecker & Peng, 1982) indicates that shoaling of the lysocline and CCD to shelf depths on a global basis during the onset of the PETM was entirely possible. That the lysocline could rise onto the shelf is certainly feasible, given the limited seafloor area between 1,000 m and the shelf-slope break, and the low wt. % CaCO_3 of siliciclastic-dominated shelf sediments, relative to deep sea sediments (Berger & Winterer, 1974); the resilience to CCD shoaling depends directly on the additional seafloor area and carbonate material exposed to corrosive waters as the CCD shoals (Delaney & Boyle, 1988). If the lysocline and CCD were to have risen to 1,000-m depth, an incrementally small addition of carbon would elevate it beyond the shelf-slope break where larger increases in shelf area per unit shoaling depth arise (i.e., the hypsometric curve is shallower). This would retard further shoaling depths on a global basis, but because the shelf covers so much area, a substantial amount of carbon would be required for the CCD to reach the middle shelf globally. Global shoaling is only projected for emission at the upper end of estimates for the PETM and a volcanic source of carbon (e.g., Gutjahr et al., 2017; Panchuk et al., 2008).

The rapid pulse of CO_2 injection required for CCD and lysocline shoaling to shelf depths may have resulted in a brief phase of surface ocean acidification. The B/Ca record from BR includes samples from the LCI but not from the level with 0% CaCO_3 (Babila et al., 2016). Moreover, thinning of coccoliths, interpreted as the potential response to surface ocean acidification, is observed in a sample from BR immediately below the LCI (O'Dea et al., 2014). Thus, it is possible that dissolution has erased the level that recorded the peak surface acidification response at BR and elsewhere.

In conclusion, the global data set, including sections from the deep ocean and other shelf sites, is consistent with shoaling of the lysocline and CCD to shelf depths. However, we stress that this is not the only possible interpretation of the data. The condensed record of deep ocean sites and the paucity of complete records allow for other explanations; as discussed, alternative interpretations also exist for shelf records. Thus, in the next section, we explore a different model whereby shoaling was a regional, not a global phenomenon.

4.2.5. The Case for Regional CCD and Lysocline Shoaling to the Continental Shelf

Eutrophication on modern shelves resulting from excessive nutrient input from rivers causes elevated microbial degradation of organic matter, leading to a combination of hypoxia and undersaturation in subsurface waters (e.g., Cai et al., 2011; Feely et al., 2008; Mathis et al., 2011) and also in the top few centimeters of the sediment column. Thus, there is a continuum between dissolution resulting from changes in saturation in bottom waters and in the sediment column during early diagenesis. Environments during the onset of the PETM on the paleoshelf of the Atlantic Coastal Plain were eutrophic (Gibbs, Bralower, et al., 2006; Lippert & Zachos, 2007; Sluijs et al., 2007; Stassen et al., 2015). Moreover, there is evidence that extreme warming during the onset of the PETM increased microbial activity (Bowen, 2013; Kopp et al., 2009). We postulate that ocean acidification on the paleoshelf of the Atlantic Coastal Plain could have been a regional phenomenon, resulting from the combination of a rapid pulse of CO_2 at the onset of the PETM and fluvially induced eutrophication. Taken a step further, the patchy distribution of carbonate both stratigraphically and geographically in the middle shelf sections is possibly a result of spatial and temporal variations in the intensity of these local and regional factors that impacted saturation. For example, the thicker LCI in the Maryland sections might be a response to their proximity to freshwater sources. Distinguishing between regional and global models for CCD and lysocline shoaling will require further study of key sections at high resolution with a multiproxy approach, including paleontological and proxy data.

5. Conclusions

Our investigation reveals a low carbonate interval within the onset of the PETM that extends across the middle and outer paleoshelf of the Salisbury Embayment on the mid-Atlantic shelf. This interval is associated with minor disconformities in the outer paleoshelf section and patchy carbonate preservation in middle paleoshelf sections. The low carbonate interval cannot be primarily explained by sediment dilution or focusing in the inner shelf or by diagenetic oxidation of organic matter or pyrite. We postulate that the CCD and lysocline shoaled to the middle shelf. The extent of shoaling of these surfaces is greater than in previous estimates but generally consistent with global compilations of carbonate data, given stratigraphic uncertainty. We propose two possible models, the first that shoaling was a global phenomenon involving rates of CO_2 addition exceeding those of published simulations with more modest shoalings. An alternative scenario

involves regional factors such as strong upwelling or eutrophication due to input of nutrients from rivers and intensified microbial activity due to warming that may have exacerbated the impact of acidification in the shallow oceans.

References in Supporting Information

These references contributed to the supporting files: Alegret et al. (2009), Aze et al. (2014), Bains et al. (1999), Bornemann et al. (2014), Bralower (2002), Bralower, Kelly, et al. (2014), Bralower, Meissner, et al. (2014), Bralower et al. (1995), Broecker and Clark (2009), Broecker (1995), Colosimo et al. (2006), Gutjahr et al. (2017), Hollis et al. (2015), Jiang and Wise (2007), Katz et al. (1999), Kelly (2002), Kelly et al. (2012), Kelly et al. (2005), Larrasoana et al. (2012), Lu et al. (1998), Norris and Röhl (1999), Panchuk et al. (2008), Penman et al. (2016), Ravizza et al. (2001), Röhl et al. (2004), Slotnick et al. (2012), Slotnick et al. (2015), Sluijs et al. (2011), Stap et al. (2009), Stassen et al. (2012), Thomas et al. (2002), Thomas et al. (1996), Thomas and Shackleton (1996), Turner et al. (2017), Zachos et al. (2005), and Zeebe et al. (2009).

Acknowledgments

This paper is dedicated to the memory of Jeff Grey, driller extraordinaire, who brought experience and dedication to the USGS Eastern Regional Drilling Crew and whose expertise was instrumental in recovering the superb quality cores at CamDor, Howards Tract, and South Dover Bridge. Colin Carney, Dyke Andreasen, Julie Anderson, Wes Auken, and Katya Bazilevskaya provided technical support. Ellen Seefelt, Rials Christenson, Louisa Lytle, Mercer Parker, Whitney Spivey Ty White, and Stephen Williamson aided in core sampling and sample preparation. Victoria Fortiz, Ashley Grey, Kalev Hantsoo, Heather Jones, Rosie Oakes, and Sheila Trampush helped in the field. Jim Browning, Appy Sluijs, and Ellen Thomas supplied samples from Millville and Bass River; Sam Gibbs generously lent us slides from Bass River. Reviews by Pete Lippert and two anonymous reviewers are greatly appreciated. This research was supported by NSF grants OCE-1415958 to Bralower and Zachos and by the USGS Land Change Science Research and Development Program. Any use of trade, firm, or product names is for descriptive purposes only and does not imply endorsement by the U.S. Government. All data are included in the supporting information or hosted in the Pangaea database (<https://www.pangaea.de/>).

References

- Alegret, L., Ortiz, S., Orue-Etxebarria, X., Bernaola, G., Baceta, J. I., Monechi, S., et al. (2009). The Paleocene–Eocene thermal maximum: New data on microfossil turnover at the Zumaia section, Spain. *PALAIOS*, 24(5), 318–328. <https://doi.org/10.2110/palo.2008.p08-057r>
- Aller, R. C. (1988). Complete oxidation of solid phase sulfides by manganese and bacteria in anoxic marine sediments. *Geochimica et Cosmochimica Acta*, 52(3), 751–765. [https://doi.org/10.1016/0016-7037\(88\)90335-3](https://doi.org/10.1016/0016-7037(88)90335-3)
- Andreasen, D., Staley, A., & Achmad, G. (2013). Maryland Coastal Plain aquifer information system: Hydrogeologic framework, Maryland Geological Survey Open-File Report 12–02–20, 121 p. Retrieved from https://www.mgs.md.gov%2Fpublications%2Freport_pages%2FOFR_12%26dash%3B02%26hyphen%3B20.html
- Archer, D., Khesghi, H., & Maier-Reimer, E. (1997). Multiple timescales for neutralization of fossil fuel CO₂. *Geophysical Research Letters*, 24(4), 405–408. <https://doi.org/10.1029/97GL00168>
- Aze, T., Pearson, P. N., Dickson, A. J., Badger, M. P. S., Bown, P. R., Pancost, R. D., et al. (2014). Extreme warming of tropical waters during the Paleocene–Eocene Thermal Maximum. *Geology*, 42(9), 739–742. <https://doi.org/10.1130/G35637.1>
- Babila, T. L., Rosenthal, Y., Wright, J. D., & Miller, K. G. (2016). A continental shelf perspective of ocean acidification and temperature evolution during the Paleocene–Eocene Thermal Maximum. *Geology*, 44(4), 275–278.
- Bains, S., Corfield, R. M., & Norris, R. D. (1999). Mechanisms of climate warming at the end of the Paleocene. *Science*, 285(5428), 724–727. <https://doi.org/10.1126/science.285.5428.724>
- Berger, W., & Winterer, E. L. (1974). Plate stratigraphy and the fluctuating carbonate line. In *Pelagic sediments: On land and under the sea* (pp. 11–48). Oxford: Blackwell.
- Berger, W. H. (1971). Sedimentation of planktonic foraminifera. *Marine Geology*, 11(5), 325–358. [https://doi.org/10.1016/0025-3227\(71\)90035-1](https://doi.org/10.1016/0025-3227(71)90035-1)
- Bornemann, A., Norris, R. D., Lyman, J. A., D'haenens, S., Groeneveld, J., Röhl, U., et al. (2014). Persistent environmental change after the Paleocene–Eocene Thermal Maximum in the eastern North Atlantic. *Earth and Planetary Science Letters*, 394, 70–81. <https://doi.org/10.1016/j.epsl.2014.03.017>
- Bowen, G. J. (2013). Up in smoke: A role for organic carbon feedbacks in Paleogene hyperthermals. *Global and Planetary Change*, 109, 18–29. <https://doi.org/10.1016/j.gloplacha.2013.07.001>
- Bralower, T. J. (2002). Evidence for surface water oligotrophy during the late Paleocene thermal maximum: Nannofossil assemblage data from Ocean Drilling Program Site 690, Maud Rise, Weddell Sea. *Paleoceanography*, 17(2), 1023. <https://doi.org/10.1029/2001PA000662>
- Bralower, T. J., Kelly, D. C., Gibbs, S., Farley, K., Eccles, L., Lindemann, T. L., & Smith, G. J. (2014). Impact of dissolution on the sedimentary record of the Paleocene–Eocene Thermal Maximum. *Earth and Planetary Science Letters*, 401, 70–82. <https://doi.org/10.1016/j.epsl.2014.05.055>
- Bralower, T. J., Meissner, K. J., Alexander, K., & Thomas, D. J. (2014). The dynamics of global change at the Paleocene–Eocene Thermal Maximum: A data-model comparison. *Geochemistry, Geophysics, Geosystems*, 15, 3830–3848. <https://doi.org/10.1002/2014GC005474>
- Bralower, T. J., & Self-Trail, J. M. (2016). Nannoplankton malformation during the Paleocene–Eocene Thermal Maximum and its paleoecological and paleoceanographic significance. *Paleoceanography*, 31, 1423–1439. <https://doi.org/10.1002/2016PA002980>
- Bralower, T. J., Thomas, D. J., Zachos, J. C., Hirschmann, M. M., Rohl, U., Sigurdsson, H., et al. (1997). High-resolution records of the late Paleocene thermal maximum and circum-Caribbean volcanism: Is there a causal link? *Geology*, 25(11), 963–966. [https://doi.org/10.1130/0091-7613\(1997\)025<0963:HRROTL>2.3.CO;2](https://doi.org/10.1130/0091-7613(1997)025<0963:HRROTL>2.3.CO;2)
- Bralower, T. J., Zachos, J. C., Thomas, E., Parrow, M., Paull, C. K., Kelly, D. C., et al. (1995). Late Paleocene to Eocene paleoceanography of the equatorial Pacific Ocean: Stable isotopes recorded at ocean drilling program site 865, Allison Guyot. *Paleoceanography*, 10(4), 841–865. <https://doi.org/10.1029/95PA01143>
- Broecker, W., & Clark, E. (2009). Ratio of coccolith CaCO₃ to foraminifera CaCO₃ in late Holocene deep sea sediments. *Paleoceanography*, 24, PA3205. <https://doi.org/10.1029/2009PA001731>
- Broecker, W. S. (1995). *The glacial world according to Wally* (Vol. 318). New York: Eldigio Press Palisades.
- Broecker, W. S., & Peng, T.-H. (1982). *Tracers in the sea*. New York: Eldigio Press.
- Cai, W.-J., Hu, X., Huang, W.-J., Murrell, M. C., Lehrter, J. C., Lohrenz, S. E., et al. (2011). Acidification of subsurface coastal waters enhanced by eutrophication. *Nature Geoscience*, 4(11), 766–770. <https://doi.org/10.1038/ngeo1297>
- Canudo, J., Keller, G., Molina, E., & Ortiz, N. (1995). Planktic foraminiferal turnover and $\delta^{13}\text{C}$ isotopes across the Paleocene–Eocene transition at Caravaca and Zumaya, Spain. *Palaeogeography, Palaeoclimatology, Palaeoecology*, 114(1), 75–100. [https://doi.org/10.1016/0031-0182\(95\)00073-U](https://doi.org/10.1016/0031-0182(95)00073-U)
- Colosimo, A., Bralower, T. J., & Zachos, J. (2006). Evidence for lysocline shoaling at the Paleocene/Eocene Thermal Maximum on Shatsky Rise, Northwest Pacific. *Proceedings Ocean Drilling Program Scientific Results*, 198, 1–36.

- Cramer, B. S., Aubry, M.-P., Miller, K. G., Olsson, R. K., Wright, J. D., & Kent, D. V. (1999). An exceptional chronologic, isotopic, and clay mineralogic record of the latest Paleocene thermal maximum, Bass River, NJ, ODP 174AX. *Bulletin de la Société géologique de France*, 170, 883–887.
- Crouch, E. M., Heilmann-Clausen, C., Brinkhuis, H., Morgans, H. E. G., Rogers, K. M., Egger, H., & Schmitz, B. (2001). Global dinoflagellate event associated with the late Paleocene thermal maximum. *Geology*, 29(4), 315–318. [https://doi.org/10.1130/0091-7613\(2001\)029<0315:GDEAWT>2.0.CO;2](https://doi.org/10.1130/0091-7613(2001)029<0315:GDEAWT>2.0.CO;2)
- Cui, Y., Kump, L. R., Ridgwell, A. J., Charles, A. J., Junium, C. K., Diefendorf, A. F., et al. (2011). Slow release of fossil carbon during the Palaeocene-Eocene Thermal Maximum. *Nature Geoscience*, 4(7), 481–485. <https://doi.org/10.1038/ngeo1179>
- Delaney, M. L., & Boyle, E. A. (1988). Tertiary paleoceanic chemical variability: Unintended consequences of simple geochemical models. *Paleoceanography*, 3(2), 137–156.
- Dickens, G. R. (2011). Down the Rabbit Hole: Toward appropriate discussion of methane release from gas hydrate systems during the Paleocene-Eocene Thermal Maximum and other past hyperthermal events. *Climate of the Past*, 7(3), 831–846. <https://doi.org/10.5194/cp-7-831-2011>
- Dickens, G. R., O'Neil, J. R., Rea, D. K., & Owen, R. M. (1995). Dissociation of oceanic methane hydrate as a cause of the carbon isotope excursion at the end of the Paleocene. *Paleoceanography*, 10(6), 965–971. <https://doi.org/10.1029/95PA02087>
- Doney, S. C., Fabry, V. J., Feely, R. A., & Kleypas, J. A. (2009). Ocean acidification: The other CO₂ problem. *Annual Review of Marine Science*, 1(1), 169–192. <http://www.ncbi.nlm.nih.gov/pubmed/21141034>. <https://doi.org/10.1146/annurev.marine.010908.163834>
- Dupuis, C., Aubry, M. P., Steurbaut, E., Berggren, W. A., Ouda, K., Magioncalda, R., et al. (2003). The Dababiya Quarry Section: Lithostratigraphy, clay mineralogy, geochemistry and paleontology. *Micropaleontology*, 49(Suppl_1), 41–59. https://doi.org/10.2113/49.Suppl_1.41
- Fabry, V. J., Seibel, B. A., Feely, R. A., & Orr, J. C. (2008). Impacts of ocean acidification on marine fauna and ecosystem processes. *ICES Journal of Marine Science*, 65, 413–432.
- Feely, R. A., Sabine, C. L., Hernandez-Ayon, J. M., Ianson, D., & Hales, B. (2008). Evidence for upwelling of corrosive “acidified” water onto the continental shelf. *Science*, 320(5882), 1490–1492. <http://www.ncbi.nlm.nih.gov/pubmed/18497259>. <https://doi.org/10.1126/science.1155676>
- Frieling, J., Gebhardt, H., Adekeye, O. A., Akande, S. O., Reichart, G. J., Middelburg, J. J. B. M., et al. (2014). The Paleocene-Eocene Thermal Maximum: Temperature and ecology in the tropics. AGU Fall Meeting Abstracts, 1, 6.
- Frieling, J., Gebhardt, H., Huber, M., Adekeye, O. A., Akande, S. O., Reichart, G.-J., et al. (2017). Extreme warmth and heat-stressed plankton in the tropics during the Paleocene-Eocene Thermal Maximum. *Science Advances*, 3(3), e1600891. <https://doi.org/10.1126/sciadv.1600891>
- Frieling, J., Svensen, H. H., Planke, S., Cramwinckel, M. J., Selnes, H., & Sluijs, A. (2016). Thermogenic methane release as a cause for the long duration of the PETM. *Proceedings of the National Academy of Sciences of the United States of America*, 113(43), 12,059–12,064. <https://doi.org/10.1073/pnas.1603348113>
- Froelich, P., Klinkhammer, G. P., Bender, M. A. A., Luedtke, N. A., Heath, G. R., Cullen, D., et al. (1979). Early oxidation of organic matter in pelagic sediments of the eastern equatorial Atlantic: Suboxic diagenesis. *Geochimica et Cosmochimica Acta*, 43(7), 1075–1090. [https://doi.org/10.1016/0016-7037\(79\)90095-4](https://doi.org/10.1016/0016-7037(79)90095-4)
- Gattuso, J.-P., Frankignoulle, M., Bourge, I., Romaine, S., & Buddemeier, R. W. (1998). Effect of calcium carbonate saturation of seawater on coral calcification. *Global and Planetary Change*, 18(1–2), 37–46. [https://doi.org/10.1016/S0921-8181\(98\)00035-6](https://doi.org/10.1016/S0921-8181(98)00035-6)
- Gazeau, F., Quiblier, C., Jansen, J. M., Gattuso, J.-P., Middelburg, J. J., & Heip, C. H. R. (2007). Impact of elevated CO₂ on shellfish calcification. *Geophysical Research Letters*, 34, L07603. <https://doi.org/10.1029/2006GL028554>
- Gibbs, S. J., Bown, P. R., Sessa, J. A., Bralower, T. J., & Wilson, P. A. (2006). Nannoplankton extinction and origination across the Paleocene-Eocene Thermal Maximum. *Science*, 314(5806), 1770–1773. <https://doi.org/10.1126/science.1133902>
- Gibbs, S. J., Bralower, T. J., Bown, P. R., Zachos, J. C., & Bybell, L. M. (2006). Shelf and open-ocean calcareous phytoplankton assemblages across the Paleocene-Eocene Thermal Maximum: Implications for global productivity gradients. *Geology*, 34(4), 233. <https://doi.org/10.1130/G22381.1>
- Gibbs, S. J., Poulton, A. J., Bown, P. R., Daniels, C. J., Hopkins, J., Young, J. R., et al. (2013). Species-specific growth response of coccolithophores to Palaeocene–Eocene environmental change. *Nature Geoscience*, 6(3), 218–222. <https://doi.org/10.1038/ngeo1719>
- Gibson, T. G., Bybell, L. M., & Mason, D. B. (2000). Stratigraphic and climatic implications of clay mineral changes around the P/E boundary of the northeastern U.S. margin. *Sedimentary Geology*, 134(1–2), 65–92. [https://doi.org/10.1016/S0037-0738\(00\)00014-2](https://doi.org/10.1016/S0037-0738(00)00014-2)
- Gibson, T. G., Bybell, L. M., & Owens, J. P. (1993). Latest Paleocene lithologic and biotic events in neritic deposits of southwestern New Jersey. *Paleoceanography*, 8(4), 495–514. <https://doi.org/10.1029/93PA01367>
- Giusberti, L., Rio, D., Agnini, C., Backman, J., Fornaciari, E., Tateo, F., & Oddone, M. (2007). Mode and tempo of the Paleocene-Eocene Thermal Maximum in an expanded section from the Venetian pre-Alps. *Geological Society of America Bulletin*, 119(3–4), 391–412. <https://doi.org/10.1130/B25994.1>
- Gutjahr, M., Ridgwell, A., Sexton, P. F., Anagnostou, E., Pearson, P. N., Pälike, H., et al. (2017). Very large release of mostly volcanic carbon during the Palaeocene–Eocene Thermal Maximum. *Nature*, 548(7669), 573–577. <https://doi.org/10.1038/nature23646>
- Handley, L., Pearson, P. N., McMillan, I. K., & Pancost, R. D. (2008). Large terrestrial and marine carbon and hydrogen isotope excursions in a new Paleocene/Eocene boundary section from Tanzania. *Earth and Planetary Science Letters*, 275(1–2), 17–25. <https://doi.org/10.1016/j.epsl.2008.07.030>
- Harris, A. D., Miller, K. G., Browning, J. V., Sugarman, P. J., Olsson, R. K., Cramer, B. S., & Wright, J. D. (2010). Integrated stratigraphic studies of Paleocene–lowermost Eocene sequences, New Jersey Coastal Plain. *Paleoceanography*, 25, PA3211. <https://doi.org/10.1029/2009PA001800>
- Heckel, P. H., Dennison, J., & Ettensohn, F. (1994). Evaluation of evidence for glacio-eustatic control over marine Pennsylvanian cyclothems in North America and consideration of possible tectonic effects. Tectonic and Eustatic Controls on Sedimentary Cycles: SEPM. *Concepts in Sedimentology and Paleontology*, 4, 65–87. <https://doi.org/10.2110/csp.94.04.0065>
- Hollis, C. J., Dickens, G. R., Field, B. D., Jones, C. M., & Strong, C. P. (2005). The Paleocene–Eocene transition at Mead Stream, New Zealand: A southern Pacific record of early Cenozoic global change. *Palaeogeography, Palaeoclimatology, Palaeoecology*, 215(3–4), 313–343. <https://doi.org/10.1016/j.palaeo.2004.09.011>
- Hollis, C. J., Hines, B. R., Littler, K., Villasante-Marcos, V., Kulhanek, D. K., Strong, C. P., et al. (2015). The Paleocene–Eocene Thermal Maximum at DSDP Site 277, Campbell Plateau, southern Pacific Ocean. *Climate of the Past*, 11(7), 1009–1025. <https://doi.org/10.5194/cp-11-1009-2015>
- Honisch, B., Ridgwell, A., Schmidt, D. N., Thomas, E., Gibbs, S. J., Sluijs, A., et al. (2012). The geological record of ocean acidification. *Science*, 335(6072), 1058–1063. <https://doi.org/10.1126/science.1208277>
- Jackson, J. B., Kirby, M. X., Berger, W. H., Bjørndal, K. A., Botsford, L. W., Bourque, B. J., et al. (2001). Historical overfishing and the recent collapse of coastal ecosystems. *Science*, 293(5530), 629–637. <https://doi.org/10.1126/science.1059199>
- Jackson, J. B. C. (2008). Ecological extinction and evolution in the brave new ocean. *PNAS*, 105(Supplement 1), 11,458–11,465. <https://doi.org/10.1073/pnas.0802812105>

- Jiang, S., & Wise, S. W. Jr. (2007). Abrupt turnover in calcareous-nannoplankton assemblages across the Paleocene/Eocene Thermal Maximum: Implications for surface-water oligotrophy over the Kerguelen Plateau, Southern Indian Ocean, U.S. Geological Survey and The National Academies Short Research Paper 24. <https://doi.org/10.3133/of2007-1047.srp3024>
- John, C. M., Bohaty, S. M., Zachos, J. C., Sluijs, A., Gibbs, S. J., Brinkhuis, H., & Bralower, T. J. (2008). North American continental margin records of the Paleocene-Eocene Thermal Maximum: Implications for global carbon and hydrological cycling. *Paleoceanography*, 23, PA2217. <https://doi.org/10.1029/2007PA001465>
- Katz, M. E., Pak, D. K., Dickens, G. R., & Miller, K. G. (1999). The source and fate of massive carbon input during the latest Paleocene thermal maximum. *Science*, 286(5444), 1531–1533. <https://doi.org/10.1126/science.286.5444.1531>
- Kelly, D. C. (2002). Response of Antarctic (ODP Site 690) planktonic foraminifera to the Paleocene-Eocene Thermal Maximum: Faunal evidence for ocean/climate change. *Paleoceanography*, 17(4), 1071. <https://doi.org/10.1029/2002pa000761>
- Kelly, D. C., Bralower, T. J., & Zachos, J. C. (1998). Evolutionary consequences of the latest Paleocene thermal maximum for tropical planktonic foraminifera. *Palaeogeography, Palaeoclimatology, Palaeoecology*, 141(1-2), 139–161. [https://doi.org/10.1016/S0031-0182\(98\)00017-0](https://doi.org/10.1016/S0031-0182(98)00017-0)
- Kelly, D. C., Bralower, T. J., Zachos, J. C., Premoli Silva, I., & Thomas, E. (1996). Rapid diversification of planktonic foraminifera in the tropical Pacific (ODP Site 865) during the late Paleocene thermal maximum. *Geology*, 24(5), 423–426. [https://doi.org/10.1130/0091-7613\(1996\)024<0423:RDOPFI>2.3.CO;2](https://doi.org/10.1130/0091-7613(1996)024<0423:RDOPFI>2.3.CO;2)
- Kelly, D. C., Nielsen, T. M., & Schellenberg, S. A. (2012). Carbonate saturation dynamics during the Paleocene–Eocene thermal maximum: Bathyal constraints from ODP sites 689 and 690 in the Weddell Sea (South Atlantic). *Marine Geology*, 303, 75–86.
- Kelly, D. C., Zachos, J. C., Bralower, T. J., & Schellenberg, S. A. (2005). Enhanced terrestrial weathering/runoff and surface ocean carbonate production during the recovery stages of the Paleocene-Eocene Thermal Maximum. *Paleoceanography*, 20, PA4023. <https://doi.org/10.1029/2005PA001163>
- Kennett, J. P., & Stott, L. D. (1991). Abrupt deep-sea warming, palaeoceanographic changes and benthic extinctions at the end of the Palaeocene. *Nature*, 353(6341), 225–229. <https://doi.org/10.1038/353225a0>
- Kent, D. V., Lanci, L., Wang, H., & Wright, J. D. (2017). Enhanced magnetization of the Marlboro Clay as a product of soil pyrogenesis at the Paleocene–Eocene boundary? *Earth and Planetary Science Letters*, 473, 303–312. <https://doi.org/10.1016/j.epsl.2017.06.014>
- Kleypas, J. A., Feely, R. A., Fabry, V. J., Langdon, C., Sabine, C. L., & Robbins, L. L. (2006). Impacts of ocean acidification on coral reefs and other marine calcifiers: A guide for future research. *Report of a workshop held 18–20 April 2005, St Petersburg, FL*, 88 pp.
- Kopp, R. E., Schumann, D., Raub, T. D., Powars, D. S., Godfrey, L. V., Swanson-Hysell, N. L., et al. (2009). An Appalachian Amazon? Magnetofossil evidence for the development of a tropical river-like system in the mid-Atlantic United States during the Paleocene-Eocene Thermal Maximum. *Paleoceanography*, 24, PA4211. <https://doi.org/10.1029/2009PA001783>
- Kump, L. R., Bralower, T. J., & Ridgwell, A. R. (2009). Ocean acidification in deep time. *Oceanography*, 22(4), 94–107. <https://doi.org/10.5670/oceanog.2009.100>
- Larrasoana, J. C., Roberts, A. P., Chang, L., Schellenberg, S. A., Gerald, J. D. F., Norris, R. D., & Zachos, J. C. (2012). Magnetotactic bacterial response to Antarctic dust supply during the Palaeocene–Eocene thermal maximum. *Earth and Planetary Science Letters*, 333, 122–133.
- Leclercq, N., Gattuso, J.-P., & Jaubert, J. (2000). CO₂ partial pressure controls the calcification rate of a coral community. *Global Change Biology*, 6(3), 329–334. <https://doi.org/10.1046/j.1365-2486.2000.00315.x>
- Lippert, P. C., & Zachos, J. C. (2007). A biogenic origin for anomalous fine-grained magnetic material at the Paleocene-Eocene boundary at Wilson Lake, New Jersey. *Paleoceanography*, 22, PA4104. <https://doi.org/10.1029/2007PA001471>
- Loutit, T. S., Hardenbol, J., Vail, P. R., & Baum, G. R. (1988). Condensed sections: The key to age determination and correlation of continental margin sequences. In C. K. Wilgus, et al. (Eds.), *Sea-Level Changes: An Integrated Approach. Special Publication-Society of Economic Paleontologists and Mineralogists* (Vol. 42, pp. 183–213).
- Lu, G., Adatte, T., Keller, G., & Ortiz, N. (1998). Abrupt climatic, oceanographic and ecologic changes near the Paleocene-Eocene transition in the deep Tethys basin: The Alademilla section, southern Spain. *Eclogae Geologicae Helveticae*, 91, 293–306.
- Lyons, S., Baczynski, A., Babila, T., Bralower, T., Hajek, E., Kump, L., et al. (2018). Paleocene–Eocene Thermal Maximum prolonged by fossil carbon oxidation. *Nature Geoscience*. <https://doi.org/10.1038/s41561-018-0277-3>
- Mathis, J. T., Cross, J. N., & Bates, N. R. (2011). The role of ocean acidification in systemic carbonate mineral suppression in the Bering Sea. *Geophysical Research Letters*, 38, L19602. <https://doi.org/10.1029/2011GL048884>
- Meister, P. (2013). Two opposing effects of sulfate reduction on carbonate precipitation in normal marine, hypersaline, and alkaline environments. *Geology*, 41(4), 499–502. <https://doi.org/10.1130/G34185.1>
- Murphy, B., Lyle, M., & Olivarez Lyle, A. (2006). Biogenic burial across the Paleocene/Eocene boundary: Ocean Drilling Program Leg 199 Site 1221. In P. A. Wilson, M. Lyle, & J. V. Firth (Eds.), *Proc. ODP, Sci. Results*, 199: College Station, TX (Ocean Drilling Program), 1–12. <https://doi.org/10.2973/odp.proc.sr.199.215.2006>
- Mutterlose, J., Linnert, C., & Norris, R. D. (2007). Calcareous nannofossils from the Paleocene–Eocene Thermal Maximum of the equatorial Atlantic (ODP Site 1260B): Evidence for tropical warming. *Marine Micropaleontology*, 65(1–2), 13–31. <https://doi.org/10.1016/j.marmicro.2007.05.004>
- Nomura, R., & Takata, H. (2005). Data report: Paleocene/Eocene benthic foraminifers, ODP Leg 199 Sites 1215, 1220, and 1221, equatorial central Pacific Ocean. In P. A. Wilson, M. Lyle, & J. V. Firth (Eds.), *Proc. ODP, Sci. Results*, 199: College Station, TX (Ocean Drilling Program), 1–34. <https://doi.org/10.2973/odp.proc.sr.199.223.2005>
- Norris, R. D., & Röhl, U. (1999). Carbon cycling and chronology of climate warming during the Palaeocene/Eocene transition. *Nature*, 401(6755), 775–778. <https://doi.org/10.1038/44545>
- O’Dea, S. A., Gibbs, S. J., Bown, P. R., Young, J. R., Poulton, A. J., Newsam, C., & Wilson, P. A. (2014). Coccolithophore calcification response to past ocean acidification and climate change. *Nature Communications*, 5, 5363. <https://doi.org/10.1038/ncomms5363>
- Orr, J. C., Fabry, V. J., Aumont, O., Bopp, L., Doney, S. C., Feely, R. A., et al. (2005). Anthropogenic Ocean acidification over the twenty-first century and its impact on calcifying organisms. *Nature*, 437(7059), 681–686. <https://doi.org/10.1038/nature04095>
- Pälike, C., Delaney, M. L., & Zachos, J. C. (2014). Deep-sea redox across the Paleocene-Eocene Thermal Maximum. *Geochemistry, Geophysics, Geosystems*, 15, 1038–1053. <https://doi.org/10.1002/2013GC005074>
- Panchuk, K., Ridgwell, A., & Kump, L. R. (2008). Sedimentary response to Paleocene-Eocene Thermal Maximum carbon release: A model-data comparison. *Geology*, 36(4), 315. <https://doi.org/10.1130/G24474A.1>
- Pandolfi, J. M., Bradbury, R. H., Saka, E., Hughes, T. P., Björndal, K. A., Cooke, R. G., et al. (2003). Global trajectories of the long-term decline of coral reef ecosystems. *Science*, 301(5635), 955–958.
- Penman, D. E., Hönisch, B., Zeebe, R. E., Thomas, E., & Zachos, J. C. (2014). Rapid and sustained surface ocean acidification during the Paleocene-Eocene Thermal Maximum. *Paleoceanography*, 29, 357–369. <https://doi.org/10.1002/2014PA002621>

- Penman, D. E., Turner, S. K., Sexton, P. F., Norris, R. D., Dickson, A. J., Boulila, S., et al. (2016). An abyssal carbonate compensation depth overshoot in the aftermath of the Palaeocene–Eocene Thermal Maximum. *Nature Geoscience*, 9(8), 575–580. <https://doi.org/10.1038/ngeo2757>
- Raffi, I., Backman, J., Zachos, J. C., & Sluijs, A. (2009). The response of calcareous nannofossil assemblages to the Paleocene Eocene Thermal Maximum at the Walvis Ridge in the South Atlantic. *Marine Micropaleontology*, 70(3–4), 201–212. <https://doi.org/10.1016/j.marmicro.2008.12.005>
- Ravizza, G., Norris, R., Blusztajn, J., & Aubry, M. P. (2001). An osmium isotope excursion associated with the late Paleocene thermal maximum: Evidence of intensified chemical weathering. *Paleoceanography*, 16(2), 155–163. <https://doi.org/10.1029/2000PA000541>
- Ridgwell, A., & Schmidt, D. N. (2010). Past constraints on the vulnerability of marine calcifiers to massive carbon dioxide release. *Nature Geoscience*, 3(3), 196–200. <https://doi.org/10.1038/ngeo755>
- Röhl, U., Brinkhuis, H., Stickley, C. E., Fuller, M., Schellenberg, S. A., Wefer, G., & Williams, G. L. (2004). Sea level and astronomically induced environmental changes in middle and late Eocene sediments from the East Tasman Plateau. *The Cenozoic Southern Ocean: tectonics, sedimentation, and climate change between Australia and Antarctica*, 151, 127–151.
- Röhl, U., Westerhold, T., Bralower, T. J., Zachos, J. C., Röhl, U., Westerhold, T., Bralower, T. J., et al. (2007). On the duration of the Paleocene–Eocene Thermal Maximum (PETM). *Geochemistry, Geophysics, Geosystems*, 8, Q12002. <https://doi.org/10.1029/2007GC001784>
- Scheibner, C., & Speijer, R. P. (2008a). Decline of coral reefs during late Paleocene to early Eocene global warming. *Earth*, 3(1), 19–26. <https://doi.org/10.5194/ee-3-19-2008>
- Scheibner, C., & Speijer, R. P. (2008b). Late Paleocene–early Eocene Tethyan carbonate platform evolution—A response to long- and short-term paleoclimatic change. *Earth-Science Reviews*, 90(3–4), 71–102. <https://doi.org/10.1016/j.earscirev.2008.07.002>
- Schmitz, B., Asaro, F., Molina, E., Monechi, S., von Salis, K., & Speijer, R. P. (1997). High-resolution iridium, $\delta^{13}\text{C}$, $\delta^{18}\text{O}$, foraminifera and nannofossil profiles across the latest Paleocene benthic extinction event at Zumaya, Spain. *Palaeogeography, Palaeoclimatology, Palaeoecology*, 133(1–2), 49–68. [https://doi.org/10.1016/S0031-0182\(97\)00024-2](https://doi.org/10.1016/S0031-0182(97)00024-2)
- Schneider-Mor, A., & Bowen, G. J. (2013). Coupled and decoupled responses of continental and marine organic-sedimentary systems through the Paleocene–Eocene Thermal Maximum, New Jersey margin, USA. *Paleoceanography*, 28, 105–115. <https://doi.org/10.1002/palo.20016>
- Seefelt, E. L., Self-Trail, J. M., & Schultz, A. P. (2015). Comparison of three preservation techniques for slowing dissolution of calcareous nannofossils in organic rich sediments. *Micropaleontology*, 61(3), 149–164.
- Self-Trail, J. M., Powars, D. S., Watkins, D. K., & Wandless, G. A. (2012). Calcareous nannofossil assemblage changes across the Paleocene–Eocene Thermal Maximum: Evidence from a shelf setting. *Marine Micropaleontology*, 92–93, 61–80. <https://doi.org/10.1016/j.marmicro.2012.05.003>
- Self-Trail, J. M., Robinson, M. M., Bralower, T. J., Sessa, J. A., Hajek, E. A., Kump, L. R., et al. (2017). Shallow marine response to global climate change during the Paleocene–Eocene Thermal Maximum, Salisbury Embayment, USA. *Paleoceanography*, 32, 710–728. <https://doi.org/10.1002/2017PA003096>
- Self-Trail, J. M., & Seefelt, E. L. (2005). Rapid dissolution of calcareous nannofossils: A case study from freshly cored sediments of the south-eastern Atlantic coastal plain. *J. Nannoplankton Research*, 27, 149–157.
- Sexton, P. F., Wilson, P. A., & Norris, R. D. (2006). Testing the Cenozoic multisite composite $\delta^{18}\text{O}$ and $\delta^{13}\text{C}$ curves: New monospecific Eocene records from a single locality, Demerara Rise (Ocean Drilling Program Leg 207). *Paleoceanography*, 21, PA2019. <https://doi.org/10.1029/2005PA001253>
- Slotnick, B. S., Dickens, G. R., Nicolo, M. J., Hollis, C. J., Crampton, J. S., Zachos, J. C., & Sluijs, A. (2012). Large-amplitude variations in carbon cycling and terrestrial weathering during the latest Paleocene and earliest Eocene: The record at Mead Stream, New Zealand. *The Journal of Geology*, 120, 487–505.
- Slotnick, B. S., Lauretano, V., Backman, J., Dickens, G. R., Sluijs, A., & Lourens, L. (2015). Early Paleogene variations in the calcite compensation depth: New constraints using old borehole sediments from across Ninetyeast Ridge, central Indian Ocean. *Climate of the Past*, 11, 473–493.
- Sluijs, A., Bijl, P. K., Schouten, S., Röhl, U., Reichert, G. J., & Brinkhuis, H. (2011). Geochemical and palynological measurements from the ODP Leg 189 at Site 1172 on the East Tasman Plateau. *PANGAEA*. <https://doi.org/10.1594/PANGAEA.756399>
- Sluijs, A., Brinkhuis, H., Crouch, E. M., John, C. M., Handley, L., Munsterman, D., et al. (2008). Eustatic variations during the Paleocene–Eocene greenhouse world. *Paleoceanography*, 23, PA4216. <https://doi.org/10.1029/2008PA001615>
- Sluijs, A., Brinkhuis, H., Schouten, S., Bohaty, S. M., John, C. M., Zachos, J. C., et al. (2007). Environmental precursors to rapid light carbon injection at the Palaeocene/Eocene boundary. *Nature*, 450(7173), 1218–1221. <https://doi.org/10.1038/nature06400>
- Stap, L., Sluijs, A., Thomas, E., & Lourens, L. (2009). Patterns and magnitude of deep sea carbonate dissolution during Eocene Thermal Maximum 2 and H2, Walvis Ridge, southeastern Atlantic Ocean. *Paleoceanography*, 24, PA1211. <https://doi.org/10.1029/2008PA001655>
- Stassen, P., Thomas, E., & Speijer, R. P. (2012). Integrated stratigraphy of the Paleocene–Eocene Thermal Maximum in the New Jersey Coastal Plain: Toward understanding the effects of global warming in a shelf environment. *Paleoceanography*, 27, PA4210. <https://doi.org/10.1029/2012PA002323>
- Stassen, P., Thomas, E., & Speijer, R. P. (2015). Paleocene–Eocene Thermal Maximum environmental change in the New Jersey Coastal Plain: Benthic foraminiferal biotic events. *Marine Micropaleontology*, 115, 1–23. <https://doi.org/10.1016/j.marmicro.2014.12.001>
- Takeda, K., & Kaiho, K. (2007). Faunal turnovers in central Pacific benthic foraminifera during the Paleocene–Eocene thermal maximum. *Palaeogeography, Palaeoclimatology, Palaeoecology*, 251(2), 175–197. <https://doi.org/10.1016/j.palaeo.2007.02.026>
- Thomas, D. J., & Bralower, T. J. (2005). Sedimentary trace element constraints on the role of North Atlantic Igneous Province volcanism in late Paleocene–early Eocene environmental change. *Marine Geology*, 217(3–4), 233–254. <https://doi.org/10.1016/j.margeo.2005.02.009>
- Thomas, D. J., Bralower, T. J., & Zachos, J. C. (1999). New evidence for subtropical warming during the late Paleocene thermal maximum: Stable isotopes from Deep Sea Drilling Project Site 527, Walvis Ridge. *Paleoceanography and Paleoclimatology*, 14(5), 561–570. <https://doi.org/10.1029/1999PA900031>
- Thomas, D. J., Zachos, J. C., Bralower, T. J., Thomas, E., & Bohaty, S. (2002). Warming the fuel for the fire: Evidence for the thermal dissociation of methane hydrate during the Paleocene–Eocene Thermal Maximum. *Geology*, 30(12), 1067–1070. [https://doi.org/10.1130/0091-7613\(2002\)030<1067:WTFFTF>2.0.CO;2](https://doi.org/10.1130/0091-7613(2002)030<1067:WTFFTF>2.0.CO;2)
- Thomas, E. (1998). Biogeography of the late Paleocene benthic foraminiferal extinction. In *Late Paleocene–Eocene climatic and biotic events in the marine and terrestrial records* (pp. 214–243). New York: Columbia University Press.
- Thomas, E. (2007). Cenozoic mass extinctions in the deep sea: What perturbs the largest habitat on Earth? *Geological Society of America Special Papers*, 424, 1–23.
- Thomas, E., & Shackleton, N. J. (1996). The Paleocene–Eocene benthic foraminiferal extinction and stable isotope anomalies. *Geological Society, London, Special Publications*, 10, 401–441.

- Thunell, R. C. (1976). Optimal indices of calcium carbonate dissolution in deep-sea sediments. *Geology*, 4(9), 525–528. [https://doi.org/10.1130/0091-7613\(1976\)4<525:OIOCCD>2.0.CO;2](https://doi.org/10.1130/0091-7613(1976)4<525:OIOCCD>2.0.CO;2)
- Trampush, S. M., & Hajek, E. A. (2017). Preserving proxy records in dynamic landscapes: Modeling and examples from the Paleocene-Eocene Thermal Maximum. *Geology*, 45(11), 967–970. <https://doi.org/10.1130/G39367.1>
- Turner, S. K., Hull, P. M., Kump, L. R., & Ridgwell, A. (2017). A probabilistic assessment of the rapidity of PETM onset. *Nature Communications*, 8(1), 353. <https://doi.org/10.1038/s41467-017-00292-2>
- Turner, S. K., & Ridgwell, A. (2016). Development of a novel empirical framework for interpreting geological carbon isotope excursions, with implications for the rate of carbon injection across the PETM. *Earth and Planetary Science Letters*, 435, 1–13. <https://doi.org/10.1016/j.epsl.2015.11.027>
- Walker, J. C., & Kasting, J. F. (1992). Effects of fuel and forest conservation on future levels of atmospheric carbon dioxide. *Palaeogeography, Palaeoclimatology, Palaeoecology*, 97(3), 151–189. [https://doi.org/10.1016/0031-0182\(92\)90207-L](https://doi.org/10.1016/0031-0182(92)90207-L)
- Winguth, A. M., Thomas, E., & Winguth, C. (2012). Global decline in ocean ventilation, oxygenation, and productivity during the Paleocene-Eocene Thermal Maximum: Implications for the benthic extinction. *Geology*, 40(3), 263–266. <https://doi.org/10.1130/G32529.1>
- Wright, J. D., & Schaller, M. F. (2013). Evidence for a rapid release of carbon at the Paleocene-Eocene Thermal Maximum. *Proceedings of the National Academy of Sciences*, 110(40), 15,908–15,913. <https://doi.org/10.1073/pnas.1309188110>
- Zachos, J. C., Rohl, U., Schellenberg, S. A., Sluijs, A., Hodell, D. A., Kelly, D. C., et al. (2005). Rapid acidification of the ocean during the Paleocene-Eocene Thermal Maximum. *Science*, 308(5728), 1611–1615. <https://doi.org/10.1126/science.1109004>
- Zachos, J. C., Wara, M. W., Bohaty, S., Delaney, M. L., Petrizzo, M. R., Brill, A., et al. (2003). A transient rise in tropical sea surface temperature during the Paleocene-Eocene Thermal Maximum. *Science*, 302(5650), 1551–1554. <https://doi.org/10.1126/science.1090110>
- Zeebe, R. E., Ridgwell, A., & Zachos, J. C. (2016). Anthropogenic carbon release rate unprecedented during the past 66 million years. *Nature Geoscience*, 9(4), 325–329. <https://doi.org/10.1038/ngeo2681>
- Zeebe, R. E., & Zachos, J. C. (2013). Long-term legacy of massive carbon input to the Earth system: Anthropocene versus Eocene. *Philosophical Transactions of the Royal Society A*, 371(2001). <https://doi.org/10.1098/rsta.2012.0006>
- Zeebe, R. E., Zachos, J. C., & Dickens, G. R. (2009). Carbon dioxide forcing alone insufficient to explain Palaeocene–Eocene Thermal Maximum warming. *Nature Geoscience*, 2(8), 576–580. <https://doi.org/10.1038/ngeo578>